

# Effective temperatures and radiation spectra for a higher-dimensional Schwarzschild–de Sitter black hole

P. Kanti and T. Pappas

*Division of Theoretical Physics, Department of Physics, University of Ioannina,  
Ioannina GR-45110, Greece*

(Received 2 June 2017; published 24 July 2017)

The absence of a true thermodynamical equilibrium for an observer located in the causal area of a Schwarzschild–de Sitter spacetime has repeatedly raised the question of the correct definition of its temperature. In this work, we consider five different temperatures for a higher-dimensional Schwarzschild–de Sitter black hole: the bare  $T_0$ , the normalized  $T_{\text{BH}}$ , and three effective ones given in terms of both the black-hole and cosmological horizon temperatures. We find that these five temperatures exhibit similarities but also significant differences in their behavior as the number of extra dimensions and the value of the cosmological constant are varied. We then investigate their effect on the energy emission spectra of Hawking radiation. We demonstrate that the radiation spectra for the normalized temperature  $T_{\text{BH}}$ —proposed by Bousso and Hawking over twenty years ago—leads to the dominant emission curve, while the other temperatures either support a significant emission rate only in a specific  $\Lambda$  regime or have their emission rates globally suppressed. Finally, we compute the bulk-over-brane emissivity ratio and show that the use of different temperatures may lead to different conclusions regarding the brane or bulk dominance.

DOI: [10.1103/PhysRevD.96.024038](https://doi.org/10.1103/PhysRevD.96.024038)

## I. INTRODUCTION

The novel theories that postulate the existence of additional spacelike dimensions in nature [1,2] with size much larger than the Planck length or even infinite have, in fact, an almost twenty-year lifetime. During that period, several aspects of gravity, cosmology and particle physics have been reconsidered in the context of these higher-dimensional theories. Black-hole solutions have been intensively studied, since the existence of extra dimensions affects both their creation and decay processes (for more information on this, one may consult the reviews in Refs. [3–14]).

The presence of the brane(s) in the model with warped extra dimensions [2] has proven so far to be an unsurmountable obstacle for the construction of analytical solutions describing regular black holes. As a result, most of the study of the decay process of a higher-dimensional black hole has been restricted in the context of the model with large extra dimensions [1], where the latter are assumed to be empty, and thus flat, and where the self-energy of the brane may be ignored compared to the black-hole mass. It is in the context of this theory that analytical expressions describing higher-dimensional black holes may be written, and the emission of particles, comprising the Hawking radiation [15], may be studied in detail.

Historically, the first solution describing a higher-dimensional, spherically symmetric black hole appeared in the 1960s, and is known as the Tangherlini solution [16]. The solution describes a higher-dimensional analogue of the Schwarzschild solution of the general theory of relativity that is formed also in the presence of a cosmological constant. Therefore, this solution constitutes in fact an

improvement of the assumption made in the context of the large-extra-dimensions scenario where the extra space is absolutely empty: here, the extra dimensions are filled with a constant distribution of energy, or with some field configuration that effectively acts as a constant distribution of energy. For a positive cosmological constant, the solution describes a higher-dimensional Schwarzschild–de Sitter black-hole spacetime.

Although the emission of Hawking radiation from higher-dimensional, spherically symmetric or rotating black holes has been extensively studied in the literature (for a partial list, see Refs. [17–37] or the aforementioned reviews [3–14]), the analyses focused on higher-dimensional Schwarzschild–de Sitter black holes are only a few. The first such work [38] contained an analytic study of the greybody factor for scalar fields propagating on the brane and in the bulk, and in addition provided exact numerical results for the radiation spectra in both emission channels. A subsequent analytic work [39] extended the aforementioned analysis by determining the next-to-leading-order term in the expansion of the greybody factor. An exact numerical study [40] then considered the emission of fields with arbitrary spin from a higher-dimensional Schwarzschild–de Sitter black hole. A series of three more recent works studied the case of a scalar field having a nonminimal coupling to the scalar curvature: the first [41] studied the case of a purely four-dimensional Schwarzschild–de Sitter black hole, the second [42] considered the scalar field either propagating in the higher-dimensional bulk or being restricted on a brane, and the third [43] provided exact numerical results for the greybody factors and radiation spectra in the same theory. A few additional works [44–48] have also appeared that

studied the greybody factors for fields propagating in the background of variants of a Schwarzschild–de Sitter black hole.

However, over the years, the question of what is the correct notion of the temperature of a Schwarzschild–de Sitter (SdS) spacetime has arisen. This spacetime contains a black hole whose event horizon sets the lower boundary of the causally connected spacetime. But it also contains a positive cosmological constant that gives rise to a cosmological horizon, the upper boundary of the causal spacetime. An observer living at any point of this causal area is never in a true thermodynamical equilibrium—the two horizons each have their own temperature, expressed in terms of their surface gravities [49,50], and thus an incessant flow of thermal energy (from the hotter black-hole horizon to the colder cosmological one) takes place at every moment. In addition, the SdS spacetime lacks an asymptotically flat limit where the black-hole parameters may be defined in a robust way. The latter problem was solved in Ref. [51], where a *normalized* black-hole temperature was proposed that made amends for the lack of an asymptotic limit. Then, assuming that the value of the cosmological constant is small and the two horizons are thus located far away from each other, one could formulate two independent thermodynamics.

Despite the above, the question of what happens as the cosmological constant becomes larger and the two horizons come closer still persisted. It was this question that gave rise to the notion of the *effective temperature* for an SdS spacetime [52–56]—namely, one that implements both the black-hole and the cosmological horizon temperatures. (For a review on this, see Ref. [57].) A number of additional works have appeared in the literature with similar or alternative approaches on the thermodynamics of de Sitter spacetimes [58–76]; however, the question of the appropriate expression of the SdS black-hole temperature still remains open.

Up to now, no work has appeared in the literature that makes a comprehensive study of the different temperatures for an SdS spacetime and compares their predictions for the corresponding Hawking radiation spectra. In fact, previous works that study the radiation spectra from a four-dimensional or higher-dimensional SdS black hole make use of either its *bare* temperature  $T_0$ , based on its surface gravity, or the normalized one  $T_{\text{BH}}$ , at will. In the context of this work, we will perform such a comprehensive study, and we will derive and compare the derived radiation spectra. We will do so not only for the aforementioned two SdS black-hole temperatures but also for three additional effective temperatures for the SdS spacetime, namely  $T_{\text{eff-}}$ ,  $T_{\text{eff+}}$ , and  $T_{\text{effBH}}$ —the use of one of the latter temperatures may be unavoidable for large values of the cosmological constant when the two horizons lie so close that the independent thermodynamics no longer hold. To address the above, we will also extend the regime of values of the

cosmological constant that has been studied in the literature so far, and consider the entire allowed regime, from a very small value up to its maximum critical value [77].

To make our analysis as general as possible, we will consider a higher-dimensional SdS spacetime. We will then study the properties of the different temperatures in terms of both the value of the cosmological constant and also the number of extra spacelike dimensions. The corresponding Hawking radiation spectra will then be produced for scalar fields, both minimally and nonminimally coupled to gravity, propagating either on our brane or in the bulk. As we will see, the different temperatures will lead to different energy emission rates for the black hole, each one with its own profile in terms of the bulk cosmological constant, the number of extra dimensions, and the value of the nonminimal coupling constant. In addition, each temperature will lead to different conclusions regarding the dominance of the brane or of the bulk.

The outline of our paper is as follows: in Sec. II, we present the theoretical framework of our analysis, the gravitational background, and the equations of motion for the scalar field, as well as the different definitions of the temperature of an SdS spacetime. In Secs. III and IV, we derive the energy emission rates for bulk and brane scalar fields having a minimal or nonminimal coupling to gravity, respectively. In Sec. V, we calculate the bulk-over-brane emissivity ratio, and in Sec. VI, we summarize our analysis and present our conclusions.

## II. THE THEORETICAL FRAMEWORK

### A. The gravitational background

We will start by considering a higher-dimensional gravitational theory with  $D = 4 + n$  total number of dimensions. The action functional of the theory will also contain a positive cosmological constant  $\Lambda$ , and will therefore read

$$S_D = \int d^{4+n}x \sqrt{-G} \left( \frac{R_D}{2\kappa_D^2} - \Lambda \right). \quad (1)$$

In the above,  $R_D$  is the higher-dimensional Ricci scalar, and  $\kappa_D^2 = 1/M_*^{2+n}$  is the higher-dimensional gravitational constant associated with the fundamental scale of gravity  $M_*$ . If we vary the above action with respect to the metric tensor  $G_{MN}$ , we obtain the Einstein field equations having the form

$$R_{MN} - \frac{1}{2} G_{MN} R_D = \kappa_D^2 T_{MN} = -\kappa_D^2 G_{MN} \Lambda, \quad (2)$$

with the only contribution to the energy-momentum tensor  $T_{MN}$  coming from the bulk cosmological constant.

The above set of equations admits a spherically symmetric solution of the form [16]

$$ds^2 = -h(r)dt^2 + \frac{dr^2}{h(r)} + r^2 d\Omega_{2+n}^2, \quad (3)$$

where  $d\Omega_{2+n}^2$  is the area of the  $(2+n)$ -dimensional unit sphere given by

$$d\Omega_{2+n}^2 = d\theta_{n+1}^2 + \sin^2\theta_{n+1}(d\theta_n^2 + \sin^2\theta_n(\cdots + \sin^2\theta_2(d\theta_1^2 + \sin^2\theta_1 d\varphi^2) \cdots)), \quad (4)$$

with  $0 \leq \varphi < 2\pi$  and  $0 \leq \theta_i \leq \pi$ , for  $i = 1, \dots, n+1$ . The radial function  $h(r)$  is found to have the explicit form [16]

$$h(r) = 1 - \frac{\mu}{r^{n+1}} - \frac{2\kappa_D^2 \Lambda r^2}{(n+3)(n+2)}. \quad (5)$$

The above gravitational background describes a  $(4+n)$ -dimensional Schwarzschild–de Sitter (SdS) spacetime, with the parameter  $\mu$  related to the black-hole mass  $M$  through the relation [78]

$$\mu = \frac{\kappa_D^2 M}{(n+2)} \frac{\Gamma[(n+3)/2]}{\pi^{(n+3)/2}}. \quad (6)$$

The horizons of the SdS black hole follow from the equation  $h(r) = 0$ —this has, in principle,  $(n+3)$  roots; however, not all of them are real and positive. In fact, the SdS spacetime may have two, one, or zero horizons, depending on the values of the parameters  $M$  and  $\Lambda$  [79]. Here, we will ensure that the values of  $M$  and  $\Lambda$  are in the regime that supports the existence of two horizons, the black-hole  $r_h$  and the cosmological one  $r_c$ , with  $r_h < r_c$ . However, the degenerate case, that results in the Nariai limit [77] in which the two horizons coincide, will also be investigated.

The higher-dimensional background (3) is seen by gravitons and particles with no standard-model quantum numbers that may propagate in the bulk. All ordinary particles, however, are restricted to live on our four-dimensional brane [1,2], and therefore propagate on a different gravitational background. The latter follows by projecting the  $(4+n)$ -dimensional background (3) on the brane, and it is realized by fixing the value of the extra angular coordinates,  $\theta_i = \pi/2$ , for  $i = 2, \dots, n+1$ . Then, we obtain the 4D line element

$$ds^2 = -h(r)dt^2 + \frac{dr^2}{h(r)} + r^2(d\theta^2 + \sin^2\theta d\varphi^2), \quad (7)$$

with the metric function  $h(r)$  preserving its form, given by Eq. (5), and thus its dependence on both the number of additional spacelike coordinates  $n$  and the value of the bulk cosmological constant  $\Lambda$ .

## B. The temperature of the Schwarzschild–de Sitter black hole

The temperature of a black hole is traditionally defined in terms of its surface gravity  $k_h$  at the location of the horizon [49,50]. The latter quantity is expressed as

$$k_h^2 = -\frac{1}{2} \lim_{r \rightarrow r_h} (D_M K_N)(D^M K^N), \quad (8)$$

where  $D_M$  is the covariant derivative and

$$K = \gamma_t \frac{\partial}{\partial t} \quad (9)$$

is the timelike Killing vector, with  $\gamma_t$  a normalization constant. In the case that the gravitational background is spherically symmetric, Eq. (8) takes the simpler form [80]

$$k_h = \frac{1}{2} \frac{1}{\sqrt{-g_{tt}g_{rr}}} |g_{tt,r}|_{r=r_h}. \quad (10)$$

When the above expression is employed for the line element (3) of a higher-dimensional Schwarzschild–de Sitter black hole, we obtain the following expression for its temperature [38,49,80]:

$$T_0 = \frac{k_h}{2\pi} = \frac{1}{4\pi r_h} [(n+1) - (n+3)\tilde{\Lambda}r_h^2], \quad (11)$$

where we have defined, for convenience, the quantity  $\tilde{\Lambda} = 2\kappa_D^2 \Lambda / (n+2)(n+3)$ , and used the condition  $f(r_h) = 0$  to replace  $\mu$  in terms of  $r_h$  and  $\tilde{\Lambda}$ .

The Schwarzschild–de Sitter spacetime is characterized, in the most generic case, by the presence of a second horizon, the cosmological horizon  $r_c$ . As a result, one may define another surface gravity  $k_c$ , this time at the location of  $r_c$ , and a temperature for the cosmological horizon [49,50], namely [38]

$$T_c = -\frac{k_c}{2\pi} = -\frac{1}{4\pi r_c} [(n+1) - (n+3)\tilde{\Lambda}r_c^2], \quad (12)$$

where care has been taken so that  $T_c$  is positive definite, since  $r_h < r_c$  [38]. The presence of the second horizon with its own temperature makes the thermodynamics of the Schwarzschild–de Sitter spacetime significantly more complicated, as compared to the cases of either asymptotically Minkowski or anti–de Sitter spacetimes [57]. The two temperatures,  $T_0$  and  $T_c$ , are in principle different; therefore, an observer located at an arbitrary point of the causal region  $r_h < r < r_c$  is not in thermodynamical equilibrium. The usual approach adopted in the literature is to make the assumption that the two horizons are located far away, and therefore each one can have its own independent thermodynamics [50,51,62]—this assumption, however, is valid

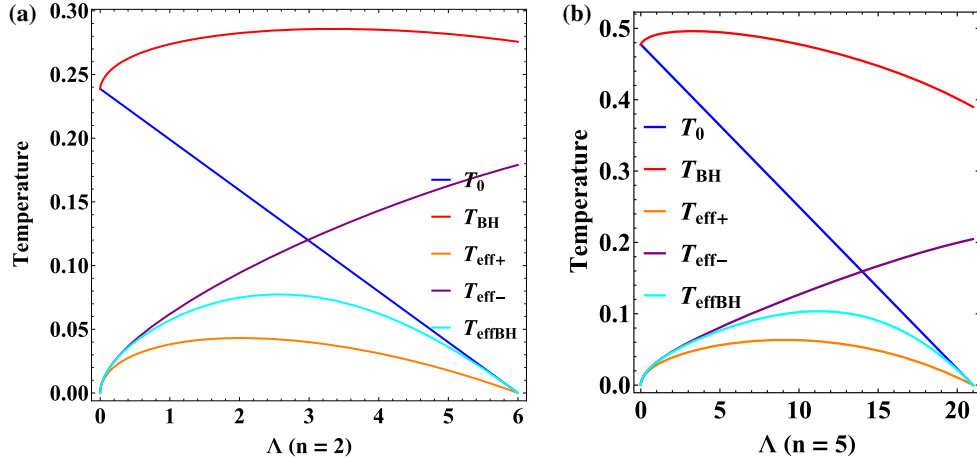


FIG. 1. Temperatures for a  $(4 + n)$ -dimensional Schwarzschild–de Sitter black hole as a function of the cosmological constant  $\Lambda$ , for (a)  $n = 2$  and (b)  $n = 5$ .

only for small values of the cosmological constant, and thus it imposes a constraint on all potential analyses.

In Ref. [51], a modified expression for the temperature of the black hole was proposed, namely

$$T_{\text{BH}} = \frac{1}{\sqrt{h(r_0)}} \frac{1}{4\pi r_h} [(n + 1) - (n + 3)\tilde{\Lambda}r_h^2], \quad (13)$$

in which a normalization factor  $\sqrt{h(r_0)}$  was introduced involving the value of the metric function at its global maximum  $r_0$ . This point follows from the condition  $h'(r) = 0$  and is given by [38]

$$r_0^{n+3} = \frac{(n + 1)\mu}{2\tilde{\Lambda}}. \quad (14)$$

There, the metric function assumes the value

$$h(r_0) = 1 - \frac{\mu}{r_0^{n+1}} - \tilde{\Lambda}r_0^2 = \frac{1}{n + 1} [(n + 1) - (n + 3)\tilde{\Lambda}r_0^2]. \quad (15)$$

The above is the maximum value that the metric function attains as it interpolates between the two zeros at the two horizons. The point  $r_0$  is the closest point that the Schwarzschild–de Sitter spacetime has to an asymptotically flat region: it is here that the effects of the black-hole and cosmological horizons cancel out and an observer can stay at rest [51]. Mathematically, the normalization factor  $\sqrt{h(r_0)}$  appears from the normalization of the Killing vector,  $K_M K^M = -1$ : this condition is satisfied in asymptotically flat spacetime for  $\gamma_t = 1$ , but at  $r = r_0$ , this factor should be  $\gamma_t = 1/\sqrt{h(r_0)}$ .

Including this normalization factor in Eq. (13) is a step forward in defining the black-hole temperature in a non-asymptotically flat spacetime; however, this factor modifies

significantly the properties of  $T_0$ . In Figs. 1(a) and 1(b), we depict the dependence of the two temperatures,  $T_0$  and  $T_{\text{BH}}$ , as a function of the cosmological constant, and for two values of the number of extra dimensions,  $n = 2$  and  $n = 5$ . For low  $n$ , as  $\Lambda$  increases,  $T_0$  monotonically decreases, in accordance with Eq. (11), whereas  $T_{\text{BH}}$  predominantly increases—the latter is caused by the variation in the value of  $h(r_0)$  that, in most of the allowed  $\Lambda$  regime, causes an enhancement in  $T_{\text{BH}}$ . For large values of  $n$ , the monotonic decrease of  $T_0$  remains unaffected, while the increase of  $T_{\text{BH}}$  holds only for the lower range of values of  $\Lambda$ . Even in this case, the value of  $T_{\text{BH}}$  is constantly larger than that of  $T_0$  (see also Ref. [40] for a similar comparison and conclusions). The two temperatures match only in the limit  $\Lambda \rightarrow 0$  when they reduce to the temperature of a higher-dimensional Schwarzschild black hole. A radically different behavior appears in the opposite limit, the Nariai or extremal limit [58,59,77]: as  $\Lambda$  approaches its maximum allowed value, the two horizons approach each other and eventually coincide, with  $r_h = r_c$ . In that limit, the combination inside the square brackets in Eq. (11), and thus  $T_0$  itself, vanishes,<sup>1</sup> a feature that is clearly shown in Fig. 1. On the contrary, in the critical limit,  $T_{\text{BH}}$  assumes an asymptotic constant value; this is caused by the fact that its numerator and denominator both tend to zero values with the ratio approaching a constant number.

In Fig. 2, we show the dependence of  $T_0$  and  $T_{\text{BH}}$  on the number of extra dimensions  $n$ , for two different fixed values of the cosmological constant,  $\Lambda = 0.1$  and  $\Lambda = 0.8$

<sup>1</sup>Although this is very difficult to prove analytically for arbitrary  $n$ , we may easily confirm it for special values of  $n$ : for  $n = 0$ , the Nariai limit is reached when  $M^2\Lambda = 1/9$  and then  $r_h^2 = 1/\Lambda$ ; for  $n = 1$ , the two horizons coincide when  $\mu\tilde{\Lambda} = 1/4$  and then  $r_h^2 = 1/(2\tilde{\Lambda})$ . In both cases, we may easily see that Eq. (11) vanishes. For higher values of  $n$ , the vanishing of Eq. (11) may be easily confirmed numerically.

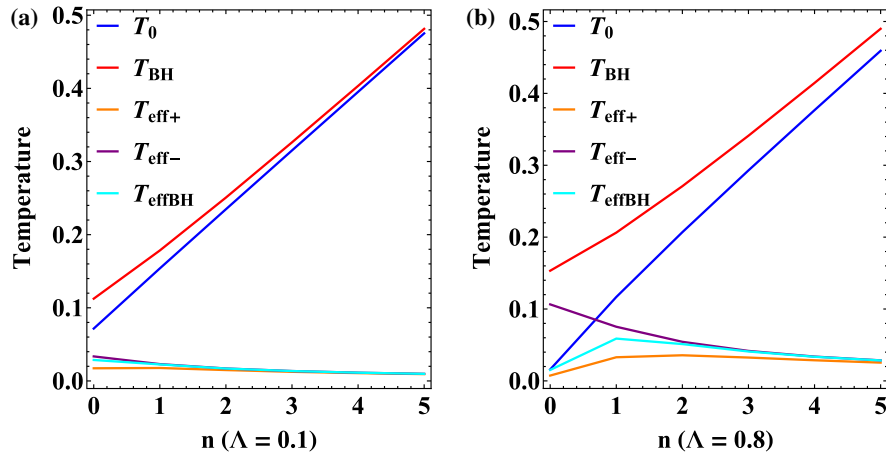


FIG. 2. Temperatures for a  $(4 + n)$ -dimensional Schwarzschild–de Sitter black hole as a function of the number of extra dimensions  $n$ , for (a)  $\Lambda = 0.1$  and (b)  $\Lambda = 0.8$ .

(we have set  $\kappa_D^2 = 1$  for simplicity; therefore  $\Lambda$  is given in units of  $r_h^{-2}$ ). We observe again that the “normalized” temperature  $T_{\text{BH}}$  remains always larger than the “bare” one  $T_0$ ; however, this dominance gets softer as  $n$  increases, and almost disappears for small values of  $\Lambda$ .

The temperature of a black hole is one of the important factors that determine the Hawking radiation emission spectra. Only a handful of works exist in the literature that study the emission of Hawking radiation from a Schwarzschild–de Sitter black hole, either four-dimensional or higher-dimensional, and these use both definitions of its temperature, Eq. (11) [41,81] or Eq. (13) [38,40,43], at will. In addition, during the recent years, the notion of the *effective temperature* of the Schwarzschild–de Sitter spacetime has emerged, that involves both temperatures  $T_0$  and  $T_c$ , in an attempt to unify the thermodynamical description of this spacetime. In the most popular of the analyses, a thermodynamical first law for a Schwarzschild–de Sitter black hole is written in which the black-hole mass plays the role of the enthalpy of the system ( $M = -H$ ), and

the cosmological constant that of the pressure ( $P = \Lambda/8\pi$ ), while the entropy is the sum of the entropies of the two horizons ( $S = S_h + S_c$ ) [52–57]. In this picture, an effective temperature emerges that has the form

$$T_{\text{eff-}} = \left( \frac{1}{T_c} - \frac{1}{T_0} \right)^{-1} = \frac{T_0 T_c}{T_0 - T_c}. \quad (16)$$

The above expression was obtained for the case of a four-dimensional Schwarzschild–de Sitter black hole. However, the arguments leading to the formulation of the aforementioned first thermodynamical law had no explicit dependence on the dimensionality of spacetime. Therefore, we expect that the functional form of the effective temperature  $T_{\text{eff-}}$  for the case of a  $(4 + n)$ -dimensional Schwarzschild–de Sitter black hole will still be given by Eq. (16), but with the individual temperatures  $T_0$  and  $T_c$ , now assuming their higher-dimensional forms, Eqs. (11) and (12). Then, the explicit form of  $T_{\text{eff-}}$  in  $D = 4 + n$  dimensions will be the following:

$$T_{\text{eff-}} = -\frac{1}{4\pi} \frac{(n+1)^2 - (n+1)(n+3)\tilde{\Lambda}(r_h^2 + r_c^2) + (n+3)^2\tilde{\Lambda}^2 r_h^2 r_c^2}{(r_h + r_c)[(n+1) - (n+3)\tilde{\Lambda} r_h r_c]}. \quad (17)$$

In the limit  $r_h \rightarrow 0$ , the above expression for the effective temperature reduces to that of the cosmological horizon  $T_c$ , as expected. However, the limit  $r_c \rightarrow \infty$  (or, equivalently,  $\tilde{\Lambda} \rightarrow 0$ ) leads to a vanishing result: the effective temperature does not interpolate between the black-hole temperature  $T_0$  and the cosmological one  $T_c$ , as one may have expected; in fact, the limit  $\Lambda \rightarrow 0$  is a particular one, since it is equivalent to a vanishing pressure of the system, that in the relevant analyses is always assumed to be positive. That is, by construction,  $T_{\text{eff-}}$  is valid for a nonvanishing cosmological constant—but this is exactly the regime

where the need for an effective temperature really emerges, since, in the limit of small  $\Lambda$ , the horizons  $r_h$  and  $r_c$  are located so far away from each other that the independent thermodynamics at the two horizons do indeed hold.

In Figs. 1 and 2, we depict also the behavior of  $T_{\text{eff-}}$  in terms of the value of the cosmological constant  $\Lambda$  and the number of extra dimensions  $n$ , respectively. The effective temperature  $T_{\text{eff-}}$  is an increasing function of  $\Lambda$ , and, similarly to the case of the normalized temperature  $T_{\text{BH}}$ , it assumes a nonvanishing constant value at the critical limit—as in the case of  $T_{\text{BH}}$ , the numerator and denominator

of Eq. (16) both go to zero with their ratio tending to a constant number. On the contrary,  $T_{\text{eff}-}$  is a decreasing function of the number of extra dimensions  $n$ .

The effective temperature  $T_{\text{eff}-}$  was found to exhibit some unphysical properties, especially in the case of charged de Sitter black holes where the aforementioned expression may take on negative values or exhibit infinite jumps at the critical point. For this reason, in Ref. [57] (see also Ref. [52]), a new expression for the effective temperature of a Schwarzschild–de Sitter spacetime was proposed, namely the following:

$$T_{\text{eff}+} = \frac{1}{4\pi} \frac{(n+1)^2 - (n+1)(n+3)\tilde{\Lambda}(r_h^2 + r_c^2) + (n+3)^2\tilde{\Lambda}^2 r_h^2 r_c^2}{(r_h - r_c)[(n+1) + (n+3)\tilde{\Lambda} r_h r_c]}. \quad (19)$$

In the limit  $r_h \rightarrow 0$ ,  $T_{\text{eff}+}$  reduces again to  $T_c$ . When  $\Lambda \rightarrow 0$ , it also exhibits the same behavior as  $T_{\text{eff}-}$  by going to zero. However, near the critical point,  $T_{\text{eff}+}$  has a distinct behavior as it vanishes instead of taking a constant value. This is in accordance with Eq. (18), where the numerator clearly approaches zero faster than the denominator. It is perhaps the vanishing of  $T_{\text{eff}+}$  near the critical point that helps to avoid the infinite jumps and makes this alternative effective temperature more physically acceptable. The complete behavior of  $T_{\text{eff}+}$  in terms of the cosmological constant is depicted in Fig. 1; its decreasing behavior in terms of  $n$  is also shown in Fig. 2.

Inspired by the above analysis, here we propose a third, alternative form for the effective temperature of a

$$T_{\text{effBH}} = -\frac{1}{4\pi} \frac{(n+1)^2 - (n+1)(n+3)\tilde{\Lambda}(r_h^2 + r_c^2) + (n+3)^2\tilde{\Lambda}^2 r_h^2 r_c^2}{(r_h \sqrt{h(r_0)} + r_c)[(n+1) - (n+3)\tilde{\Lambda} r_h r_c]}. \quad (21)$$

The above definition shares many characteristics with the effective temperature  $T_{\text{eff}-}$ : it also reduces to  $T_c$  when  $r_h \rightarrow 0$ , and it vanishes in the limit  $\Lambda \rightarrow 0$ . But it also exhibits the same attractive behavior near the critical point as  $T_{\text{eff}+}$  by going to zero; this is due to the fact that, as we approach the critical point,  $T_{\text{BH}}$  in Eq. (20) is a constant while  $T_c$  vanishes. The complete profile of  $T_{\text{effBH}}$  as a function of the cosmological constant is depicted in Fig. 1, while its similar behavior in terms of  $n$ , compared to the other effective temperatures, is shown in Fig. 2. Observing Fig. 1, it is interesting to note that  $T_{\text{effBH}}$  matches  $T_{\text{eff}-}$  over an extended low- $\Lambda$  regime, and then coincides with  $T_0$  in the high- $\Lambda$  regime.<sup>2</sup>

<sup>2</sup>One may wonder whether an alternative effective temperature could be defined along the lines of Eq. (20) but with a normalized temperature for the cosmological horizon too, i.e.  $T_{c\text{BH}} = T_c / \sqrt{h(r_0)}$ . As one may see, such a temperature would have a similar behavior to  $T_{\text{eff}-}$  in the small- $\Lambda$  regime but would have an ill-defined behavior near the critical point where it diverges.

$$T_{\text{eff}+} = \left( \frac{1}{T_c} + \frac{1}{T_0} \right)^{-1} = \frac{T_0 T_c}{T_0 + T_c}. \quad (18)$$

The above proposal was characterized as an *ad hoc* one, that would follow from an analysis similar to that leading to  $T_{\text{eff}-}$ , in which the entropy of the system would be the difference of the entropies of the two horizons, i.e.  $S = S_c - S_h$ , instead of their sum. In the higher-dimensional case, the aforementioned alternative effective temperature has the explicit form

Schwarzschild–de Sitter spacetime. Its functional form is the following:

$$T_{\text{effBH}} = \left( \frac{1}{T_c} - \frac{1}{T_{\text{BH}}} \right)^{-1} = \frac{T_{\text{BH}} T_c}{T_{\text{BH}} - T_c}, \quad (20)$$

and it matches the form of  $T_{\text{eff}-}$ , but with the normalized black-hole temperature  $T_{\text{BH}}$  in the place of the bare one  $T_0$ . Our proposal may be considered as an equally *ad hoc* one compared to that of Eq. (18); however,  $T_{\text{effBH}}$  would follow from exactly the same analysis that gave rise to  $T_{\text{eff}-}$  (with  $S = S_h + S_c$ ), with the only difference being the consideration that the “correct” black-hole temperature, due to the absence of asymptotic flatness, is  $T_{\text{BH}}$  instead of  $T_0$ . Its explicit form in a spacetime with  $D = 4 + n$  dimensions is

### III. HAWKING RADIATION FOR MINIMALLY COUPLED SCALAR FIELDS

In the previous section, we examined in detail the characteristics of two temperatures for the Schwarzschild–de Sitter black hole, the bare temperature  $T_0$  and the normalized one  $T_{\text{BH}}$  as well as three effective temperatures for the Schwarzschild–de Sitter spacetime,  $T_{\text{eff}-}$ ,  $T_{\text{eff}+}$ , and  $T_{\text{effBH}}$ , to which the SdS black hole belongs. In this section, we proceed to derive and compare the radiation spectra for scalar fields emitted by the SdS black hole, for each one of the aforementioned five temperatures.

Our analysis will focus on the higher-dimensional case and will present radiation spectra for scalar fields emitted both on the brane and in the bulk. To this end, we also need the greybody factor for brane and bulk scalar fields propagating in the SdS background. These have been derived analytically, in the limit of a small cosmological constant, in Ref. [42] and numerically, for arbitrary values

of  $\Lambda$ , in Ref. [43]. Since here we are interested in deriving the form of the spectra for the complete range of  $\Lambda$ , we will use the exact results derived in Ref. [43]. For the sake of completeness, we will briefly review the method for calculating the scalar greybody factors in a SdS spacetime—for more information, interested readers may consult Ref. [43].

We will start from the emission of scalar fields on the brane. The equation of motion of a free, massless scalar field minimally coupled to gravity and propagating in the brane background (7) has the form

$$\frac{1}{\sqrt{-g}} \partial_\mu \left( \sqrt{-g} g^{\mu\nu} \partial_\nu \Phi \right) = 0. \quad (22)$$

If we assume a factorized ansatz for the field, i.e.  $\Phi(t, r, \theta, \varphi) = e^{-i\omega t} R(r) Y(\theta, \varphi)$ , where  $Y(\theta, \varphi)$  are the usual scalar spherical harmonics, we obtain a radial equation for the function  $R(r)$  of the form:

$$\frac{1}{r^2} \frac{d}{dr} \left( h r^2 \frac{dR}{dr} \right) + \left[ \frac{\omega^2}{h} - \frac{l(l+1)}{r^2} \right] R = 0. \quad (23)$$

As was shown in Ref. [43], in the near-horizon regime, the above equation takes the form of a hypergeometric equation. Its solution, when expanded in the limit  $r \rightarrow r_h$ , takes the form of an ingoing free wave, namely

$$R_{\text{BH}} \simeq A_1 f^{\alpha_1} = A_1 e^{-i(\omega r_h/A_h) \ln f}, \quad (24)$$

where  $A(r) = (n+1) - (n+3)\tilde{\Lambda}r^2$  and  $A_h = A(r=r_h)$ . Also,  $f$  is a new radial variable defined through the relation

$$r \rightarrow f(r) = \frac{h(r)}{1 - \tilde{\Lambda}r^2}. \quad (25)$$

For simplicity, we may appropriately choose the arbitrary constant  $A_1$  so that

$$R_{\text{BH}}(r_h) = 1. \quad (26)$$

The above expression serves as a boundary condition for the numerical integration of Eq. (23). The second boundary condition comes from the near-horizon value of the first derivative of the radial function (24), for which we obtain [43]

$$\left. \frac{dR_{\text{BH}}}{dr} \right|_{r_h} \simeq -\frac{i\omega}{h(r)}. \quad (27)$$

Near the cosmological horizon, the radial equation (23) again takes the form of a hypergeometric differential equation whose general solution, in the limits  $r \rightarrow r_c$  and  $f \rightarrow 0$ , is written as [42,43]

$$R_C \simeq B_1 e^{-i(\omega r_c/A_c) \ln f} + B_2 e^{i(\omega r_c/A_c) \ln f}. \quad (28)$$

In the above,  $A_c = A(r=r_c)$  and  $B_{1,2}$  are the amplitudes of the ingoing and outgoing free waves. Then, the greybody factor, or equivalently the transmission probability, for the scalar field is given by

$$|A|^2 = 1 - \left| \frac{B_2}{B_1} \right|^2. \quad (29)$$

The  $B_{1,2}$  amplitudes are found by integrating numerically Eq. (23), starting close to the black-hole horizon, i.e. from  $r = r_h + \epsilon$ , where  $\epsilon = 10^{-6} - 10^{-4}$ , and proceeding towards the cosmological horizon (again, for more information on this, see Ref. [43]). The exact numerical analysis demonstrated that for a minimally coupled, massless scalar field propagating on the brane, the greybody factor is enhanced over the whole energy regime as the cosmological constant  $\Lambda$  increases.

Having at our disposal the exact values of the greybody factor  $|A|^2$ , we may now proceed to derive the differential energy emission rate for brane scalars. This is given by the expression [3,18,38]

$$\frac{d^2 E}{dt d\omega} = \frac{1}{2\pi} \sum_l \frac{N_l |A|^2 \omega}{\exp(\omega/T) - 1}, \quad (30)$$

where  $\omega$  is the energy of the emitted particle, and  $N_l = 2l + 1$  the multiplicity of states that, due to the spherical symmetry, have the same angular-momentum number [82]. Also,  $T$  is the temperature of the black hole—this will be taken to be equal to  $T_0, T_{\text{BH}}, T_{\text{eff-}}, T_{\text{eff+}}$  and  $T_{\text{effBH}}$  in order to derive the corresponding radiation spectra. As was demonstrated in Ref. [43], the dominant modes of the scalar field are the ones with the lowest values of  $l$ —in fact, all modes higher than the  $l = 7$  mode have negligible contributions to the total emission rate.

In Fig. 3, we depict the differential energy emission rates for a higher-dimensional Schwarzschild–de Sitter black hole for the case of  $n = 2$  and for four different values of the bulk cosmological constant ( $\Lambda = 0.8, 2, 4, 5$ ). For the first small value of  $\Lambda$ , all the effective temperatures have an almost vanishing value; therefore, the corresponding spectra are significantly suppressed—it is the two black-hole temperatures,  $T_0$  and  $T_{\text{BH}}$ , that lead to significant emission rates, with the latter dominating over the former in accordance to the behavior presented in Fig. 1. As  $\Lambda$  increases to the value of 2, the effective temperatures, and their corresponding spectra, start becoming important; at the same time, the emission spectrum for the bare temperature  $T_0$  is suppressed, whereas the one for the normalized  $T_{\text{BH}}$  is enhanced. For  $\Lambda = 4$  and 5, finally, the radiation spectrum for  $T_{\text{BH}}$  is further enhanced, while the one for  $T_{\text{eff-}}$  has also become important—it is these two temperatures that tend to a constant, nonvanishing value at the

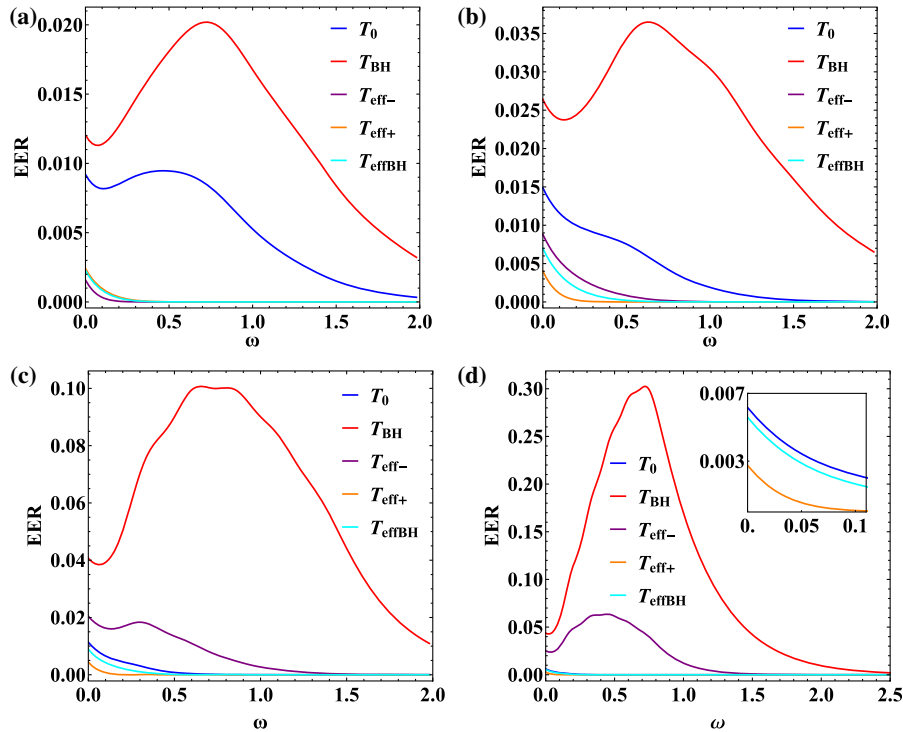


FIG. 3. Energy emission rates for scalar fields on the brane from a six-dimensional ( $n = 2$ ) Schwarzschild–de Sitter black hole for different temperatures  $T$ , and for (a)  $\Lambda = 0.8$ , (b)  $\Lambda = 2$ , (c)  $\Lambda = 4$ , and (d)  $\Lambda = 5$  (in units of  $r_h^{-2}$ ).

critical limit; on the contrary, all three remaining temperatures,  $T_0$ ,  $T_{\text{eff}+}$ , and  $T_{\text{effBH}}$ , tend to zero, thus causing a suppression to the corresponding spectra.

Let us also note that the traditional shape of the energy emission curves—starting from zero and reaching a maximum value before vanishing again—is severely distorted. The presence of the cosmological constant leads to a nonvanishing asymptotic value of the greybody factor in the limit  $\omega \rightarrow 0$  [38,39,41–43] given by

$$|A^2| = \frac{4r_h^2 r_c^2}{(r_c^2 + r_h^2)^2} + \mathcal{O}(\omega). \quad (31)$$

The above holds for the case of minimally coupled, massless scalar fields propagating in the brane background, and it leads to a significant emission rate of extremely soft, low-energetic particles—this feature is evident in all plots of Fig. 3. In addition, when the temperature employed has a small value, like the effective temperatures in the low- and intermediate- $\Lambda$  regimes or  $T_0$ ,  $T_{\text{eff}+}$ , and  $T_{\text{effBH}}$  near the critical limit, the emission curve never reaches a maximum at an energy larger than zero; rather, it exhibits only the “tail” and monotonically decreases towards zero.

The case of an even higher-dimensional Schwarzschild–de Sitter black hole with  $n = 5$  is shown in Fig. 4. A similar behavior to the one presented in the case of  $n = 2$  is also observed here: for low values of  $\Lambda$ , the radiation spectra for all effective temperatures are suppressed; as  $\Lambda$  increases,

they get moderately enhanced, while for large values of  $\Lambda$  only the one for  $T_{\text{eff}-}$  takes up significant values. The radiation spectrum for the bare temperature  $T_0$  starts at its highest values for small  $\Lambda$  and is constantly suppressed as the value of the cosmological constant increases. The radiation spectrum for the normalized black-hole temperature  $T_{\text{BH}}$  is the one that dominates over the whole  $\Lambda$  regime—even in the high- $\Lambda$  regime, where  $T_{\text{BH}}$  is suppressed with  $\Lambda$  according to Fig. 1(b), the compensating enhancement of the greybody factor [43] causes the overall increase of the differential energy emission rate.

Let us also study the emission of scalar fields from a higher-dimensional Schwarzschild–de Sitter black hole in the bulk. The equation of motion of a free, massless field propagating in the bulk is also given by the covariant equation (22), but with the projected metric tensor  $g_{\mu\nu}$  of Eq. (7) being replaced by the higher-dimensional one  $G_{MN}$  given in Eq. (3). Assuming again a factorized form  $\Phi(t, r, \theta_i, \varphi) = e^{-i\omega t} R(r) \tilde{Y}(\theta_i, \varphi)$ , where  $\tilde{Y}(\theta_i, \varphi)$  are the hyperspherical harmonics [83], we obtain the following radial equation [42]:

$$\frac{1}{r^{n+2}} \frac{d}{dr} \left( h r^{n+2} \frac{dR}{dr} \right) + \left[ \frac{\omega^2}{h} - \frac{l(l+n+1)}{r^2} \right] R = 0. \quad (32)$$

The above differential equation may be again analytically solved for small  $\Lambda$  [42], but for the purpose of comparing the radiation spectra over the entire  $\Lambda$  regime, we turn again

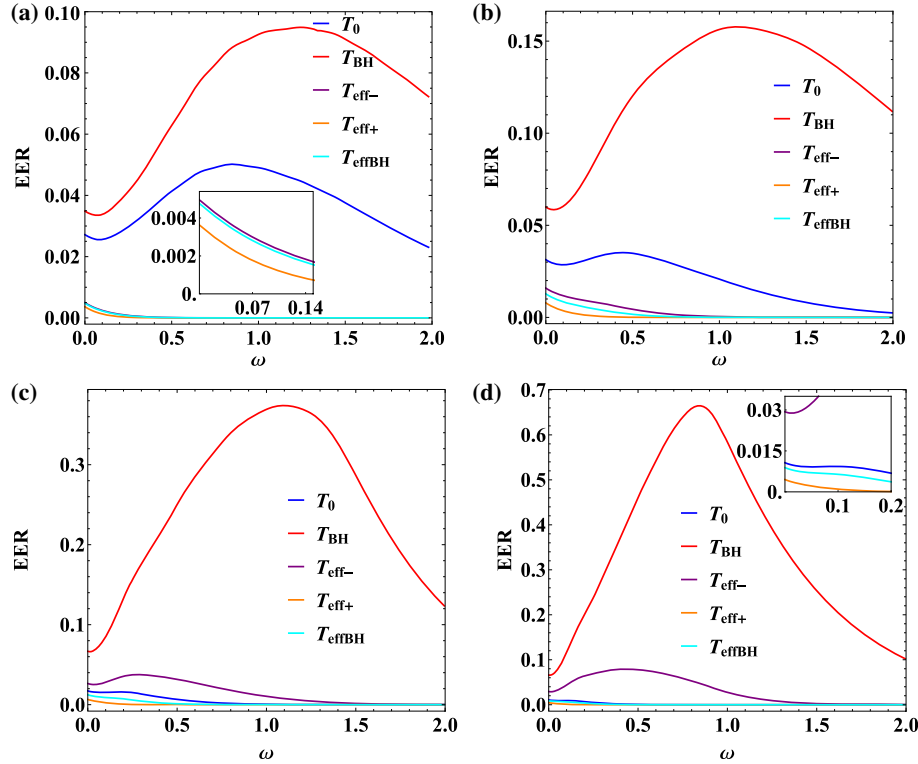


FIG. 4. Energy emission rates for scalar fields on the brane from a nine-dimensional ( $n = 5$ ) Schwarzschild–de Sitter black hole for different temperatures  $T$ , and for (a)  $\Lambda = 4$ , (b)  $\Lambda = 10$ , (c)  $\Lambda = 16$ , and (d)  $\Lambda = 18$  (in units of  $r_h^{-2}$ ).

to numerical integration. This has been performed in Ref. [43] by following an analysis similar to the one for brane scalar fields. The asymptotic solutions of Eq. (32) near the black-hole and cosmological horizons take similar forms to the brane ones, with their expanded forms (24) and (28) being identical. The same boundary conditions (26) and (27) were used for the numerical integration from the black-hole to the cosmological horizon. The exact value of the greybody factor for bulk scalar fields, for arbitrary values of the particle and spacetime parameters, was again derived via Eq. (29), and found to be an increasing function of the bulk cosmological constant.

In Fig. 5, we display the differential energy emission rates for bulk scalar fields emitted by a six-dimensional ( $n = 2$ ) SdS black hole, and for four different values of the cosmological constant. Similarly to the behavior observed in the case of brane emission, the radiation spectrum for the normalized temperature  $T_{\text{BH}}$  is the one that dominates and gets enhanced as  $\Lambda$  increases, under the combined effect of the temperature and greybody profiles. The spectrum for the bare temperature  $T_0$ , starting from significant values for low  $\Lambda$ , is again monotonically suppressed as  $\Lambda$  increases, approaching its maximum critical value. The spectra for all effective temperatures start from extremely low values, and only the one for  $T_{\text{eff-}}$  manages to reach non-negligible values—this takes place only near the critical limit where  $T_{\text{eff-}}$  acquires a constant value. If we allow for a larger

value of the number of extra dimensions, i.e.  $n = 5$ , the general behavior of the emission curves remains the same, as can be seen from the plots in Fig. 6, drawn for four different values of the cosmological constant. Here, the additional suppression of all effective temperatures with  $n$  even more keeps the corresponding radiation spectra at low values.

Also in the bulk, all emission curves tend to a non-vanishing value in the limit  $\omega \rightarrow 0$ . This is again due to the nonzero asymptotic value of the greybody factor in the very low-energy regime. However, this value for bulk emission is [38]

$$|A^2| = \frac{4(r_h r_c)^{(n+2)}}{(r_c^{n+2} + r_h^{n+2})^2} + \mathcal{O}(\omega). \quad (33)$$

The above expression is suppressed with the number of extra dimensions  $n$ , and this is the reason why this feature is more difficult to discern in the nine-dimensional emission curves of Fig. 6 compared to the six-dimensional ones of Fig. 5—it is nevertheless visible in the zoom-in plots that have been added in Fig. 6.

The numerical analysis performed in the context of the present work serves not only as a comparison of the radiation emission curves when different expressions for the temperature of the SdS spacetime are used, but also as

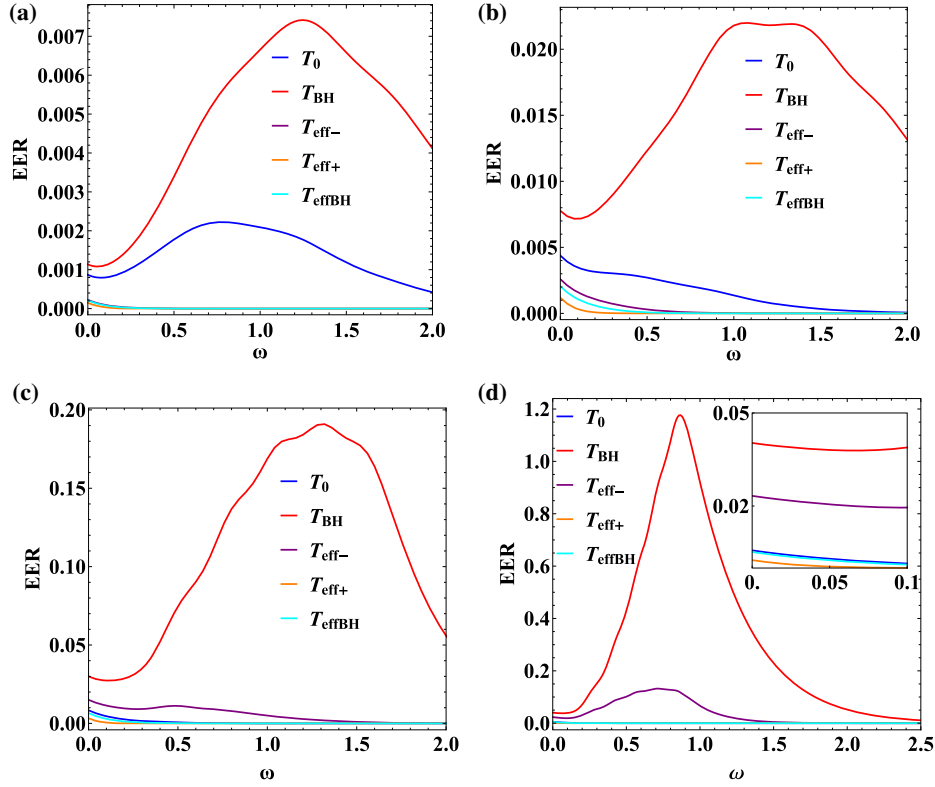


FIG. 5. Energy emission rates for scalar fields in the bulk from a six-dimensional ( $n = 2$ ) Schwarzschild–de Sitter black hole for different temperatures  $T$ , and for (a)  $\Lambda = 0.8$ , (b)  $\Lambda = 2$ , (c)  $\Lambda = 4$ , and (d)  $\Lambda = 5$  (in units of  $r_h^{-2}$ ).

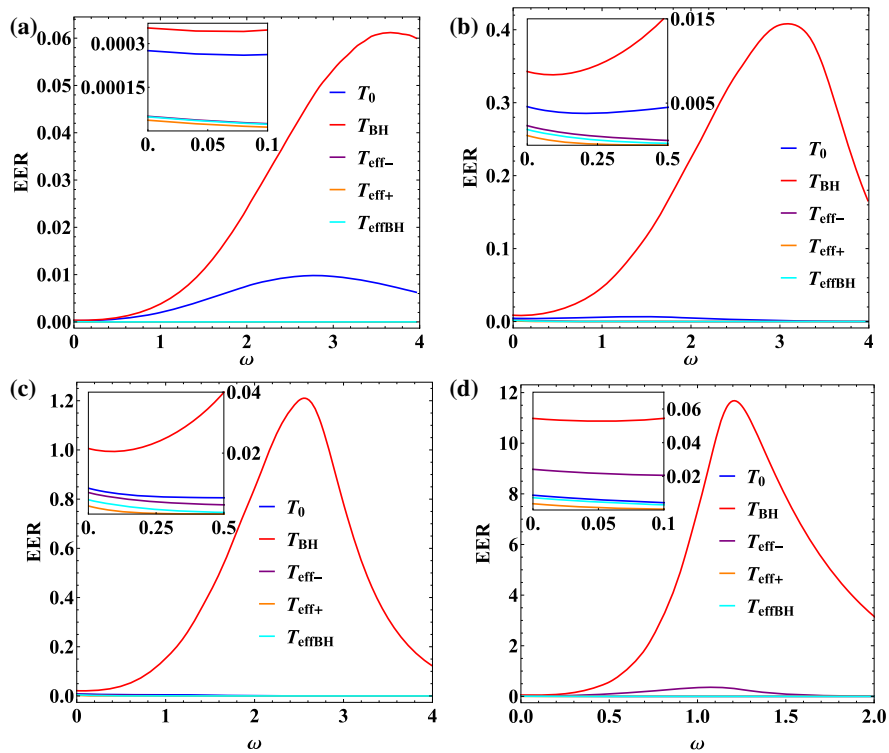


FIG. 6. Energy emission rates for scalar fields in the bulk from a nine-dimensional ( $n = 5$ ) Schwarzschild–de Sitter black hole for different temperatures  $T$ , and for (a)  $\Lambda = 4$ , (b)  $\Lambda = 10$ , (c)  $\Lambda = 13$ , and (d)  $\Lambda = 18$  (in units of  $r_h^{-2}$ ).

an extension to the previous results obtained in Ref. [43] where the normalized temperature  $T_{\text{BH}}$  was employed. There, exact results for the radiation spectra were produced, but the range of values of the cosmological constant was much more restricted, i.e.  $\Lambda \in [0.01, 0.3]$ ; therefore, the regime of large values of  $\Lambda$ , including the critical limit, was never studied. Here, we have performed a thorough analysis of the  $\Lambda$  regime for all different temperatures, and thus we have the complete picture of how the corresponding radiation spectra behave as a function of the value of the cosmological constant.

Overall, after having performed both the brane and the bulk analysis, we may conclude that it is the black-hole temperatures  $T_0$  and  $T_{\text{BH}}$  that lead to Hawking radiation emission curves with the typical shape—i.e., starting from a low value in the low-energy regime, rising to a maximum height, and then slowly dying out in the high-energy regime. In fact, even the  $T_0$  spectrum loses this typical shape as  $\Lambda$  increases. Of the effective temperatures, only  $T_{\text{eff-}}$  manages to mimic this behavior, and does so only close to the critical limit.

If we focus on the most typical radiation spectra, i.e. the ones derived for the normalized temperature  $T_{\text{BH}}$ , we could comment on some additional features that emerge from the more thorough study, in terms of the  $\Lambda$  regime, performed in the present work. Our current results have confirmed the enhancement of the corresponding radiation spectra in terms of both the number of extra dimensions  $n$  and the value of the cosmological constant, as found in Ref. [43]. As  $\Lambda$  increases, the nonzero asymptotic value of each curve in the limit  $\omega \rightarrow 0$  is enhanced, thus increasing the probability of the emission of very low-energy particles. In addition, for large values of  $n$ , as  $\Lambda$  increases, all emission curves, for brane and bulk propagation alike, show a significant shift of the peak of the curves towards the lower part of the spectrum. Therefore, we may conclude that the presence of a cosmological constant gives a significant boost to both low- and intermediate-energy free, massless scalar particles, and it does so more effectively the larger the number of extra dimensions is.

Finally, in Ref. [43], it was found that for  $\Lambda$  in the regime  $[0.01, 0.3]$ , the brane emission channel for free, massless scalar fields is always dominant compared to the bulk channel. Here, we observe that for larger values of  $\Lambda$  the situation is radically changed: even for small values of  $n$ , i.e.  $n = 2$ , the comparison of the vertical axes of the plots of Figs. 3 and 5 reveals that the bulk emission curve has surpassed, by a factor of 2, the brane one, for values of  $\Lambda$  larger than 4. As the dimensionality of spacetime increases, the bulk dominance becomes more important: for  $n = 5$ , the comparison of the vertical axes of the plots of Figs. 4 and 6 now tells us that the bulk dominates over the brane for values of  $\Lambda > 10$ , i.e., for more than half the allowed regime of values of the cosmological constant, by a factor that ranges between 3 and 20.

#### IV. HAWKING RADIATION SPECTRA FOR NONMINIMALLY COUPLED SCALAR FIELDS

In this section, we will consider the case of scalar particles propagating either on the brane or in the bulk and having a nonminimal coupling to gravity. This coupling is realized through a quadratic function  $\xi\Phi^2$ , where  $\xi$  is a constant, multiplying the appropriate scalar curvature (with the value  $\xi = 0$  corresponding to the minimal coupling). The reason for studying such a theory is twofold: First, the presence of the nonminimal coupling acts as an effective mass term for the scalar field; therefore the effect of the mass on the radiation spectra may thus be studied. Second, for large values of the coupling constant  $\xi$ , it has been found that the enhancement of the radiation spectra with the cosmological constant—for the normalized temperature  $T_{\text{BH}}$ , which was also evident in the results of the previous section—changes to a suppression in the low-energy and intermediate-energy regimes [43]. It would thus be interesting to see what the effect of the nonminimal coupling would be on the radiation spectra over the complete  $\Lambda$  regime and for different temperatures.

For a scalar field propagating in the bulk, its higher-dimensional action would read

$$S_\Phi = -\frac{1}{2} \int d^{4+n}x \sqrt{-G} [\xi \Phi^2 R_D + \partial_M \Phi \partial^M \Phi], \quad (34)$$

where  $G_{MN}$  is again the higher-dimensional metric tensor defined in Eq. (3), and  $R_D$  is the corresponding curvature given by the expression

$$R_D = \frac{2(n+4)}{n+2} \kappa_D^2 \Lambda \quad (35)$$

in terms of the bulk cosmological constant. The equation of motion of the bulk scalar field now reads

$$\frac{1}{\sqrt{-G}} \partial_M (\sqrt{-G} G^{MN} \partial_N \Phi) = \xi R_D \Phi, \quad (36)$$

or, more explicitly,

$$\frac{1}{r^{n+2}} \frac{d}{dr} \left( h r^{n+2} \frac{dR}{dr} \right) + \left[ \frac{\omega^2}{h} - \frac{l(l+n+1)}{r^2} - \xi R_D \right] R = 0. \quad (37)$$

In the above we have decoupled the radial part of the equation by considering the same factorized ansatz, namely  $\Phi(t, r, \theta_i, \varphi) = e^{-i\omega t} R(r) \tilde{Y}(\theta_i, \varphi)$ , as in the previous section.

The action functional for a scalar field propagating on the brane background and having also a quadratic, non-minimal coupling to the scalar curvature will have a form similar to Eq. (34). However, now the metric tensor  $G_{MN}$  will be replaced by the projected-on-the-brane one  $g_{\mu\nu}$

given in Eq. (7), and the higher-dimensional Ricci scalar  $R_D$  by the four-dimensional one  $R_4$  that is found to be [42]

$$R_4 = \frac{24\kappa_D^2\Lambda}{(n+2)(n+3)} + \frac{n(n-1)\mu}{r^{n+3}}. \quad (38)$$

The equation for the radial part of the brane-localized, nonminimally coupled scalar field then follows from Eq. (37) by setting  $n = 0$  and changing  $R_D$  with  $R_4$ , and it reads

$$\frac{1}{r^2} \frac{d}{dr} \left( hr^2 \frac{dR}{dr} \right) + \left[ \frac{\omega^2}{h} - \frac{l(l+1)}{r^2} - \xi R_4 \right] R = 0. \quad (39)$$

Both equations (37) and (39) were solved analytically in Ref. [42] and numerically in Ref. [43]. As it is clear from both equations, the nonminimal coupling term acts as an effective mass term; therefore, any increase in the coupling function  $\xi$  causes a suppression to the radiation spectra, in accordance with previous studies of massive scalar fields [84–87]. In addition, in Ref. [43], it was found that as  $\xi$  exceeds the value of approximately 0.3, any increase in the value of the cosmological constant causes a suppression in the low and intermediate parts of the spectrum.

In the light of the above, here we will consider a value for the nonminimal coupling constant well beyond that critical value—namely, we will choose  $\xi = 1$ . We will also study

the complete  $\Lambda$  regime and compute the radiation spectra for all five temperatures:  $T_0$ ,  $T_{\text{BH}}$ ,  $T_{\text{eff-}}$ ,  $T_{\text{eff+}}$ , and  $T_{\text{effBH}}$ . We will use again the exact numerical results for the brane and bulk greybody factors, that follow from an analysis identical to that in the minimal-coupling case—although the coupling constant  $\xi$  modifies the form of the effective potentials that the brane and bulk scalar fields have to overcome to reach infinity [42], it has no effect in the asymptotic regimes of the two horizons; therefore, the asymptotic solutions (24) and (28) as well as the boundary conditions (26) and (27) remain the same.

Starting from the emission of nonminimally coupled scalar fields on the brane, in Fig. 7 we depict the differential energy emission rates for a six-dimensional SdS black hole, and for the values  $\Lambda = 2, 2.8, 4,$  and  $5$  of the bulk cosmological constant. We first note that, in the presence of  $\xi$ , the emission curves have returned to their typical shape: as was found in Refs. [41,42], and confirmed also here, the nonminimal coupling destroys the nonzero asymptotic limit of the scalar greybody factor in the low-energy limit; as a result, all emission curves emanate from zero in the low-energy regime. Moreover, the larger the value of  $\xi$ , the later in terms of  $\omega$  the emission curves rise above the zero value, in accordance with the effect that the mass of the scalar particle has on the spectra [86,87]. Also, by comparing the vertical axes of Figs. 3(b) and 3(c) with those of Figs. 7(a) and 7(c), respectively, we observe that the radiation spectra in the nonminimal case are indeed

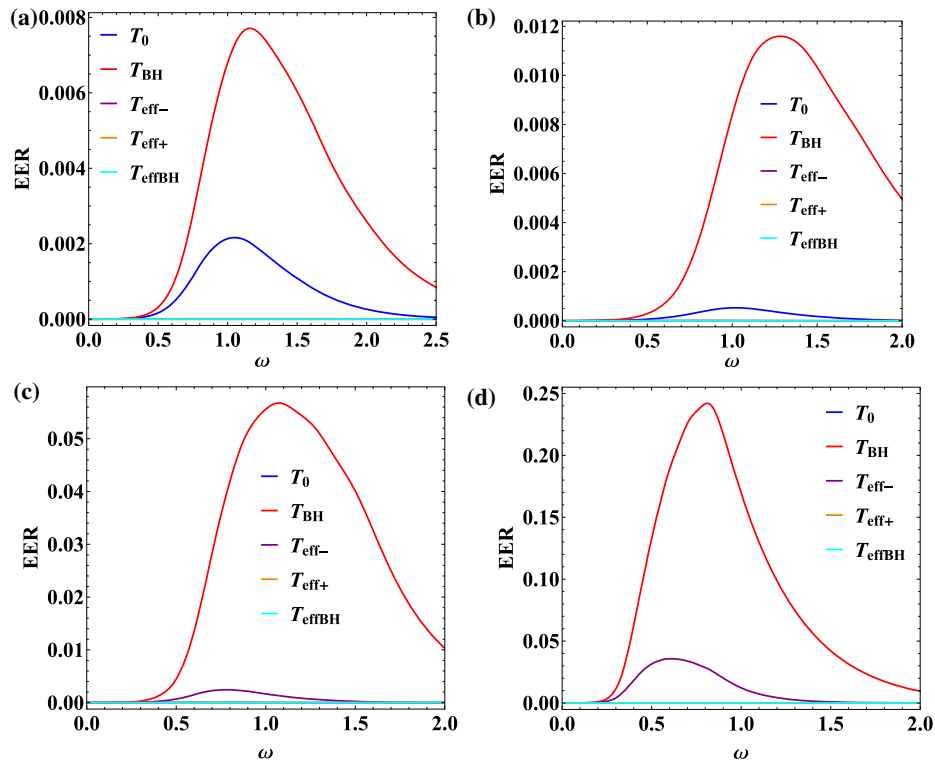


FIG. 7. Energy emission rates for nonminimally coupled brane scalar fields, with  $\xi = 1$ , from a six-dimensional ( $n = 2$ ) SdS black hole for different temperatures  $T$ , and for (a)  $\Lambda = 2$ , (b)  $\Lambda = 2.8$ , (c)  $\Lambda = 4$ , and (d)  $\Lambda = 5$  (in units of  $r_h^{-2}$ ).

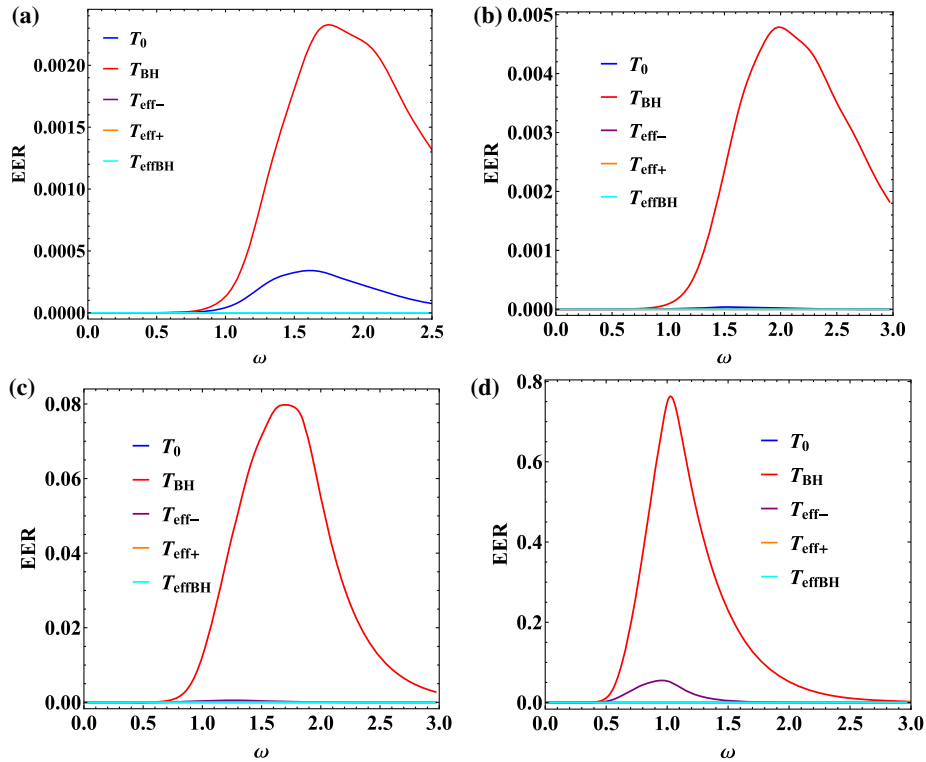


FIG. 8. Energy emission rates for nonminimally coupled bulk scalar fields, with  $\xi = 1$ , from a six-dimensional ( $n = 2$ ) SdS black hole for different temperatures  $T$ , and for (a)  $\Lambda = 2$ , (b)  $\Lambda = 2.8$ , (c)  $\Lambda = 4$ , and (d)  $\Lambda = 5$  (in units of  $r_h^{-2}$ ).

significantly suppressed, in accordance with the previous discussion.

This suppression is due to the fact that the greybody factors for both brane and bulk scalar fields decrease with any increase in the nonminimal coupling constant  $\xi$ , and therefore are common to the radiation spectra for the different temperatures. As a result, the inclusion of the nonminimal coupling does not modify the general picture drawn in the previous section. However, some of the radiation spectra are more sensitive to the changes brought by the presence of the nonminimal coupling. For example, in Fig. 3, drawn for the minimal-coupling case, we observe that, for the three effective temperatures and  $T_0$ , the maxima of all emission curves are located at the very low-energy limit; the relatively small magnitude of these temperatures, compared to that of  $T_{\text{BH}}$ , combined with the enhanced value of the greybody factor for ultrasoft particles, makes the emission of low-energetic particles much more favorable for the black hole. When the nonminimal coupling is introduced, the emission of soft particles becomes disfavored, and the radiation spectra for the aforementioned four temperatures are significantly suppressed. The radiation spectrum for the normalized temperature  $T_{\text{BH}}$  is also suppressed; however, its relatively large value allows also for the significant emission of higher-energetic particles, and these are not significantly affected by the nonminimal coupling. As a result, the relative

enhancement of the  $T_{\text{BH}}$  radiation spectrum compared to the remaining ones is extended by the nonminimal coupling. As the critical limit is approached, only the  $T_{\text{eff-}}$  spectrum manages again to reach comparable values due to its asymptotic, nonzero value in that regime.

A similar behavior is observed also in the case where the number of extra dimensions takes larger values. We have performed the same analysis for  $n = 5$ , and found that all emission curves for nonminimally coupled brane scalar fields return again to their typical shape and thus have the emission of low-energy particles suppressed. For small values of  $\Lambda$ , and due to the enhancement with  $n$  that characterizes both  $T_0$  and  $T_{\text{BH}}$  (see Fig. 2), the difference in the corresponding two radiation spectra is smaller compared to the case with  $n = 2$ . As  $\Lambda$  increases, however, the  $T_0$  radiation spectrum is constantly suppressed, reaching a negligible value at the critical limit. Of the effective temperature, only  $T_{\text{eff-}}$  manages to support a relatively significant spectrum, and that is realized very close to the critical limit.

We now turn to the case of the emission of nonminimally coupled scalar fields emitted in the bulk. The radiation spectra for the different temperatures and for the case with  $n = 2$  are now depicted in Fig. 8, again for the value  $\xi = 1$  and for the same four values of the cosmological constant. A similar picture emerges also here: the  $T_0$  radiation spectrum is significant only in the low- $\Lambda$  regime, and

$T_{\text{eff-}}$  becomes important near the critical limit, while the other two radiation spectra, for  $T_{\text{eff+}}$  and  $T_{\text{effBH}}$ , fail to acquire any significant value in any  $\Lambda$  regime. The radiation spectrum for  $T_{\text{BH}}$  is the one that dominates over the whole energy regime and for the entire  $\Lambda$  range. The same behavior is observed also for  $n = 5$ .

Let us finally note that the dominance of the bulk emission channel in the large- $\Lambda$  regime [43] is confirmed also in the case of nonminimal coupling and even for models with a small number of extra dimensions. As the comparison of the vertical axes of Figs. 7 and 8 reveals, the differential energy emission rate in the bulk exceeds that on the brane as soon as  $\Lambda$  becomes approximately larger than 3, and it stays dominant for the remaining half of the allowed range.

### V. BULK-OVER-BRANE RELATIVE EMISSIVITIES

A final question that we would like to address in this section is that of the effect of the different temperatures on the total emissivities in the bulk and on the brane, and more particularly on the bulk-over-brane emissivity ratio. In our previous work [43], we calculated the total power emitted by the SdS black hole over the whole frequency range in both the brane and bulk channels by employing the Bousso-Hawking  $T_{\text{BH}}$  normalization for the temperature. Here, we generalize this analysis to cover all five temperatures— $T_0$ ,  $T_{\text{BH}}$ ,  $T_{\text{eff-}}$ ,  $T_{\text{eff+}}$ , and  $T_{\text{effBH}}$ —and compare the corresponding results. We also extend our previous study by considering the whole range of values for the bulk cosmological constant, from a vanishing value up to its critical limit.

The quantity of interest, namely the ratio of the total power emitted in the bulk over the corresponding total power on the brane, for the case with  $n = 2$  and for four different values of the coupling constant  $\xi$ —i.e.,  $\xi = 0, 0.5, 1, 2$ —is presented in Tables I–IV. The five columns of each table give the total ratio for five values of the cosmological constant that span the entire allowed range: i.e., for  $\Lambda = 0.3, 1, 2, 4, 5$ . Let us see first how the change in the value of  $\Lambda$  affects our results. For small values of  $\Lambda$ , and independently of the value of  $\xi$ , the brane emission channel clearly dominates over the bulk one; however, as  $\Lambda$  increases, the bulk emission channel gradually becomes more and more important. This is due to the fact that for an increasing cosmological constant, the bulk emission curves move to the right, thus allowing for the emission of a larger number of high-energetic particles compared to that on the brane, but also, the maximum height of the bulk curves soon overtakes that of the brane curves by a factor of 3. For the  $T_{\text{BH}}$  and  $T_{\text{eff-}}$  temperatures, which retain a significant value near the critical limit, the bulk-over-brane ratio well exceeds unity, thus rendering the bulk channel the dominant one in the emission process of the black hole—the tendency of  $T_{\text{BH}}$  to overturn the power ratio in favor of the

TABLE I. Bulk-over-brane total emissivity for  $n = 2$  and  $\xi = 0$ .

$\Lambda \rightarrow$	0.3	1	2	4	5
$T_0$	0.259 268	0.304 247	0.402 190	0.663 547	0.781 833
$T_{\text{BH}}$	0.338 245	0.506 324	0.798 603	1.929 660	3.247 190
$T_{\text{eff-}}$	0.032 997	0.132 329	0.319 508	0.860 880	2.071 590
$T_{\text{eff+}}$	0.032 507	0.125 599	0.298 895	0.717 772	0.884 068
$T_{\text{effBH}}$	0.032 950	0.130 510	0.309 000	0.669 669	0.792 598

TABLE II. Bulk-over-brane total emissivity for  $n = 2$  and  $\xi = 0.5$ .

$\Lambda \rightarrow$	0.3	1	2	4	5
$T_0$	0.281 627	0.220 836	0.160 691	0.089 933	0.067 954
$T_{\text{BH}}$	0.369 359	0.450 873	0.629 061	1.617 200	2.962 410
$T_{\text{eff-}}$	0.003 762	0.012 441	0.038 311	0.432 708	1.710 000
$T_{\text{eff+}}$	0.003 424	0.008 841	0.014 009	0.019 979	0.021 436
$T_{\text{effBH}}$	0.003 725	0.011 167	0.022 578	0.046 074	0.052 124

TABLE III. Bulk-over-brane total emissivity for  $n = 2$  and  $\xi = 1$ .

$\Lambda \rightarrow$	0.3	1	2	4	5
$T_0$	0.286 455	0.165 240	0.089 413	0.032 550	0.020 609
$T_{\text{BH}}$	0.380 420	0.387 464	0.500 779	1.364 060	2.704 060
$T_{\text{eff-}}$	0.001 233	0.003 214	0.011 410	0.279 735	1.433 260
$T_{\text{eff+}}$	0.001 140	0.002 529	0.003 787	0.005 227	0.005 582
$T_{\text{effBH}}$	0.001 222	0.002 907	0.005 497	0.012 099	0.013 918

TABLE IV. Bulk-over-brane total emissivity for  $n = 2$  and  $\xi = 2$ .

$\Lambda \rightarrow$	0.3	1	2	4	5
$T_0$	0.280 978	0.099 559	0.035 998	0.007 446	0.003 698
$T_{\text{BH}}$	0.382 963	0.287 373	0.331 984	1.002 190	2.289 020
$T_{\text{eff-}}$	0.000 222	0.000 471	0.001 935	0.138 896	1.045 890
$T_{\text{eff+}}$	0.000 216	0.000 410	0.000 580	0.000 778	0.000 828
$T_{\text{effBH}}$	0.000 221	0.000 438	0.000 738	0.001 767	0.002 089

bulk channel was already anticipated by the results of Ref. [43]. The only exception to the above behavior is the one exhibited by the bare temperature  $T_0$ : the enhancement of the bulk-over-brane ratio with  $\Lambda$  is observed only in the case of minimal coupling, whereas this ratio decreases for all values  $\xi \neq 0$ , as  $\Lambda$  increases towards its critical value. We may interpret this as the result of the disappearance of the low-energy modes as soon as the coupling constant  $\xi$  takes a nonvanishing value: the emission curves for  $T_0$  have their maxima in the low-energy regime and are thus mostly affected when these are banned from the emission spectrum—according to our results, this

change affects the bulk channel more than the brane one, causing the suppression of the bulk-over-brane ratio.

If we now turn our attention to the role of the non-minimal coupling constant  $\xi$  in the value of the bulk-over-brane ratio, we find that the overall behavior is a suppression of this quantity as  $\xi$  increases. This behavior holds for almost all values of the cosmological constant apart from the lower part of its allowed regime where, in contrast, the bulk-over-brane ratio exhibits an enhancement without, however, exceeding unity. On the other hand, despite the suppression with  $\xi$ , the bulk-over-brane ratio retains values above unity when  $\Lambda$  tends to its critical limit.

When we increase the number of the extra dimensions, all the above effects become amplified. In Tables V–VIII,

we display the value of the bulk-over-brane ratio for the case with  $n = 5$ , for the same four values of the non-minimal coupling constant  $\xi$  and for five indicative values of the bulk cosmological constant, i.e.  $\Lambda = 1, 4, 10, 13,$  and  $18$ , that again span the entire allowed regime. The dominance of the bulk channel over the brane one for  $T_{\text{BH}}$  and  $T_{\text{eff-}}$ , as  $\Lambda$  approaches its critical limit, is now much more prominent, with the overall energy emitted in the bulk surpassing the one emitted on the brane by a factor even larger than 10. The suppression of the energy ratio as  $\xi$  increases is also obvious here, but again this suppression does not prevent the bulk from becoming the dominant channel at the critical limit. What is different in this case from the  $n = 2$  case is that the enhancement with  $\xi$  for

TABLE V. Bulk-over-brane total emissivity for  $n = 5$  and  $\xi = 0$ .

$\Lambda \rightarrow$	1	4	10	13	18
$T_0$	0.296 070	0.299 653	0.357 216	0.422 606	0.584 868
$T_{\text{BH}}$	0.419 245	0.818 056	2.578 580	4.629 670	14.182 30
$T_{\text{eff-}}$	0.000 267	0.010 603	0.140 588	0.328 066	4.192 670
$T_{\text{eff+}}$	0.000 265	0.010 319	0.137 045	0.291 825	0.658 816
$T_{\text{effBH}}$	0.000 267	0.010 549	0.134 856	0.273 098	0.559 205

TABLE VI. Bulk-over-brane total emissivity for  $n = 5$  and  $\xi = 0.5$ .

$\Lambda \rightarrow$	1	4	10	13	18
$T_0$	0.468 836	0.288 097	0.099 659	0.054 591	0.016 835
$T_{\text{BH}}$	0.641 474	0.841 435	1.770 690	3.060 490	11.199 70
$T_{\text{eff-}}$	$3.152 \times 10^{(-6)}$	0.000 090	0.002 028	0.018 275	2.231 760
$T_{\text{eff+}}$	$2.898 \times 10^{(-6)}$	0.000 071	0.000 552	0.000 923	0.001 500
$T_{\text{effBH}}$	$3.139 \times 10^{(-6)}$	0.000 086	0.000 938	0.002 127	0.005 982

TABLE VII. Bulk-over-brane total emissivity for  $n = 5$  and  $\xi = 1$ .

$\Lambda \rightarrow$	1	4	10	13	18
$T_0$	0.664 875	0.248 447	0.040 067	0.015 499	0.002 610
$T_{\text{BH}}$	0.890 165	0.778 299	1.195 190	2.049 140	9.026 680
$T_{\text{eff-}}$	$3.679 \times 10^{(-7)}$	0.000 007	0.000 200	0.003 575	1.293 840
$T_{\text{eff+}}$	$3.956 \times 10^{(-7)}$	0.000 006	0.000 054	0.000 095	0.000 164
$T_{\text{effBH}}$	$3.683 \times 10^{(-7)}$	0.000 007	0.000 080	0.000 187	0.000 616

TABLE VIII. Bulk-over-brane total emissivity for  $n = 5$  and  $\xi = 2$ .

$\Lambda \rightarrow$	1	4	10	13	18
$T_0$	1.162 700	0.179 527	0.009 087	0.002 170	0.000 160
$T_{\text{BH}}$	1.509 360	0.632 852	0.585 960	1.010 350	6.207 500
$T_{\text{eff-}}$	0.000 274	$1.054 \times 10^{(-6)}$	$6.508 \times 10^{(-6)}$	0.000 305	0.514 108
$T_{\text{eff+}}$	0.000 299	$1.653 \times 10^{(-6)}$	$1.827 \times 10^{(-6)}$	$3.402 \times 10^{(-6)}$	$6.292 \times 10^{(-6)}$
$T_{\text{effBH}}$	0.000 275	$1.033 \times 10^{(-6)}$	$2.328 \times 10^{(-6)}$	$5.573 \times 10^{(-6)}$	0.000 022

small values of the cosmological constant, noted also in the case with  $n = 2$ , is now adequate to cause the dominance of the bulk channel over the brane one for the bare  $T_0$  and normalized  $T_{\text{BH}}$  temperatures—for the latter temperature, this effect was also observed in Ref. [43].

## VI. CONCLUSIONS

Over the years, the study of the thermodynamics of the Schwarzschild–de Sitter spacetime has proven to be a challenging task. The existence of two different horizons, the black-hole and the cosmological one—each with its own temperature expressed in terms of its surface gravity—results in the absence of a true thermodynamical equilibrium. On the other hand, the absence of an asymptotically flat limit led to the formulation of a normalized temperature for the black hole [51] more than two decades ago. Both problems become more severe in the limit of a large cosmological constant when the two horizons are located so close to each other that the argument of the two independent thermodynamics, valid at the two horizons, comes into question. As a result, the notion of the effective temperature of the SdS spacetime was proposed [53–56] that implements both the black-hole and the cosmological horizon temperatures.

In the context of the present work, we have focused on the case of the higher-dimensional Schwarzschild–de Sitter black hole, and have formed a set of five different temperatures: the bare black-hole temperature  $T_0$  based on its surface gravity, the normalized black-hole temperature  $T_{\text{BH}}$ , and three effective temperatures for the SdS spacetime,  $T_{\text{eff-}}$ ,  $T_{\text{eff+}}$ , and  $T_{\text{effBH}}$ —the latter three are inspired by four-dimensional analyses, where the cosmological constant plays the role of the pressure of the system, and are combinations of the black-hole and cosmological horizon temperatures. We have first studied the dependence of the aforementioned temperatures on the value of the cosmological constant, as this is varied from zero to its maximum allowed value, set by the critical limit where the two horizons coincide. In the limit of a vanishing cosmological constant, the black-hole temperatures  $T_0$  and  $T_{\text{BH}}$  reduce to the temperature of an asymptotically flat, higher-dimensional Schwarzschild black hole as expected; on the other hand, all three effective temperatures tend to zero, an artificially ill behavior due to the fact that  $\Lambda$  (or, equivalently, the pressure of the system) is not allowed to vanish. In the opposite limit, that of the critical value, it is the normalized  $T_{\text{BH}}$  and effective  $T_{\text{eff-}}$  temperatures that have a common behavior reaching a nonvanishing asymptotic value; the other three temperatures all vanish in the same limit. We then examined the dependence of the temperatures on the number of extra dimensions. Here, the five temperatures were found to fall again into two categories: the black-hole temperatures  $T_0$  and  $T_{\text{BH}}$  are both enhanced with  $n$ , while all effective temperatures predominantly are

suppressed. Overall, the normalized  $T_{\text{BH}}$  temperature was found to be the dominant one for all values of  $\Lambda$  and  $n$ .

The set of five temperatures was then used to derive the Hawking radiation spectra for a free, massless scalar field propagating both on the brane and in the bulk. We considered the cases where the number of extra dimensions had a small ( $n = 2$ ) and a large ( $n = 5$ ) value: in each case, we chose four different values for the cosmological constant that covered the allowed regime from zero to the critical value. For both brane and bulk radiation spectra, the emission curves closely followed the behavior of the temperatures: for small  $\Lambda$ , the emission curves for all effective temperatures were significantly suppressed, while the ones for the black-hole temperatures were the dominant ones. As  $\Lambda$  increased, the emission rate for the bare  $T_0$  started to become suppressed, while the one for the effective  $T_{\text{eff-}}$  started to become important. Near the critical limit, it is the two temperatures  $T_{\text{BH}}$  and  $T_{\text{eff-}}$  with the nonvanishing values that lead to the dominant emission curves. It is worth noting that the two effective temperatures  $T_{\text{eff+}}$  and  $T_{\text{effBH}}$  support a non-negligible emission rate only for intermediate values of the cosmological constant, where they favor the emission of very low-energy scalar particles. The emission rate for the normalized temperature  $T_{\text{BH}}$  is one that constantly rises as  $\Lambda$  gradually increases, being clearly the dominant one: for  $n = 2$ , the peak of the emission curve on the brane for  $T_{\text{BH}}$  rises to a height that is 2 times larger than that for  $T_0$  in the low- $\Lambda$  regime and 5 times larger than that for  $T_{\text{eff-}}$  in the high- $\Lambda$  regime; these factors increase even more as  $n$  increases, or when we study the bulk emission channel.

For the case of a minimally coupled scalar field, all emission curves were found to have nonzero asymptotic values at the very low part of the spectrum due to the well-known behavior of the greybody factor both on the brane and in the bulk. As a result, a significant number of soft particles are expected to be emitted; in fact, for the three effective temperatures  $T_{\text{eff-}}$ ,  $T_{\text{eff+}}$ ,  $T_{\text{effBH}}$  (for small values of values of  $\Lambda$ ) and for  $T_0$  (for large values of  $\Lambda$ ), this is where the peak of the emission curves is located. When the nonminimal coupling to the scalar curvature is turned on, the emission curves for all five temperatures resume their usual shape. The general behavior regarding the comparative strength of the emission curves for the different temperatures observed in the case of the minimal coupling holds also here. The emission curve for the normalized temperature  $T_{\text{BH}}$  is again the dominant one over the entire  $\Lambda$  regime, with only the emission curves for  $T_0$  and  $T_{\text{eff-}}$  reaching significant values at low and large values of  $\Lambda$ , respectively.

The exact analysis performed in the context of this work serves not only as a comparison of the radiation spectra, which follow by using different temperatures for the Schwarzschild–de Sitter spacetime, but also as a source of information regarding their behavior as the cosmological

constant varies from a very small value to the largest allowed one at the critical limit. The complete radiation spectra reveal that as  $\Lambda$  increases, the emission of energy from the black hole along the brane and bulk channels very quickly become comparable, and even for low values of the number of extra dimensions, the bulk emission eventually dominates over the brane one. The exact total emissivities that were calculated in Sec. V demonstrated exactly this effect: apart from the case of  $T_0$  when  $\xi \neq 0$ , the bulk-over-brane ratio exhibits a significant enhancement as  $\Lambda$  increases and, in fact, renders the bulk channel the dominant emission channel of the SdS black hole for the temperatures  $T_{\text{BH}}$  and  $T_{\text{eff-}}$ —i.e., for the temperatures that retain a nonvanishing value near the critical limit. In addition, when the number of extra dimensions is large enough, the bulk is found to dominate over the brane even for values of  $\Lambda$  much lower than its critical limit, as long as the value of the nonminimal coupling constant  $\xi$  is large

enough; in this case, the bulk dominance is obtained also for the bare temperature  $T_0$ .

In conclusion, choosing a particular form for the temperature of an SdS black hole—i.e., the bare, the normalized, or an effective one—plays a paramount role in the form of the obtained radiation spectra. Some of the suggested temperatures fail even to produce a significant emission rate; others lead to an emission only for very small or very large values of the bulk cosmological constant. Our results clearly reveal that the normalized temperature  $T_{\text{BH}}$ , the one that makes amends for the absence of an asymptotically flat limit in a Schwarzschild–de Sitter spacetime, is the one that produces the most robust radiation spectra over the entire regime of the bulk cosmological constant.

### ACKNOWLEDGMENT

T. P. would like to thank the Alexander S. Onassis Public Benefit Foundation for financial support.

- 
- [1] N. Arkani-Hamed, S. Dimopoulos, and G.R. Dvali, The hierarchy problem and new dimensions at a millimeter, *Phys. Lett. B* **429**, 263 (1998); Phenomenology, astrophysics and cosmology of theories with sub-millimeter dimensions and TeV scale quantum gravity, *Phys. Rev. D* **59**, 086004 (1999); I. Antoniadis, N. Arkani-Hamed, S. Dimopoulos, and G.R. Dvali, New dimensions at a millimeter to a Fermi and superstrings at a TeV, *Phys. Lett. B* **436**, 257 (1998).
- [2] L. Randall and R. Sundrum, Large Mass Hierarchy from a Small Extra Dimension, *Phys. Rev. Lett.* **83** (1999) 3370; An Alternative to Compactification, *Phys. Rev. Lett.* **83** (1999) 4690.
- [3] P. Kanti, Black holes in theories with large extra dimensions: A review, *Int. J. Mod. Phys. A* **19**, 4899 (2004).
- [4] M. Cavaglia, Black hole and brane production in TeV gravity: A review, *Int. J. Mod. Phys. A* **18**, 1843 (2003).
- [5] G.L. Landsberg, Black holes at future colliders and in cosmic rays, *Eur. Phys. J. C* **33**, S927 (2004).
- [6] A. S. Majumdar and N. Mukherjee, Braneworld black holes in cosmology and astrophysics, *Int. J. Mod. Phys. D* **14**, 1095 (2005).
- [7] S. C. Park, Black holes and the LHC: A review, *Prog. Part. Nucl. Phys.* **67**, 617 (2012).
- [8] B. Webber, Black holes at accelerators, eConf **C0507252**, T030 (2005).
- [9] A. Casanova and E. Spallucci, TeV mini black hole decay at future colliders, *Classical Quantum Gravity* **23**, R45 (2006).
- [10] P. Kanti, Black holes at the LHC, *Lect. Notes Phys.* **769**, 387 (2009).
- [11] P. Kanti, Footprints of higher-dimensional decaying black holes, *Romanian Journal of Physics* **57**, 879 (2012).
- [12] E. Winstanley, Hawking radiation from rotating brane black holes, [arXiv:0708.2656](https://arxiv.org/abs/0708.2656).
- [13] P. Kanti, Brane-world black holes, *J. Phys. Conf. Ser.* **189**, 012020 (2009).
- [14] P. Kanti and E. Winstanley, Hawking radiation from higher-dimensional black holes, *Fundam. Theor. Phys.* **178**, 229 (2015).
- [15] S. W. Hawking, Particle creation by black holes, *Commun. Math. Phys.* **43**, 199 (1975).
- [16] F.R. Tangherlini, Schwarzschild field in  $n$  dimensions and the dimensionality of space problem, *Nuovo Cimento* **27**, 636 (1963).
- [17] P. Kanti and J. March-Russell, Calculable corrections to brane black hole decay: I. The scalar case, *Phys. Rev. D* **66**, 024023 (2002); Calculable corrections to brane black hole decay: II. Greybody factors for spin 1/2 and 1, *Phys. Rev. D* **67**, 104019 (2003).
- [18] C.M. Harris and P. Kanti, Hawking radiation from a  $(4+n)$ -dimensional black hole: Exact results for the Schwarzschild phase, *J. High Energy Phys.* **10** (2003) 014.
- [19] A. S. Cornell, W. Naylor, and M. Sasaki, Graviton emission from a higher-dimensional black hole, *J. High Energy Phys.* **02** (2006) 012; V. Cardoso, M. Cavaglia, and L. Gualtieri, Black Hole Particle Emission in Higher-Dimensional Spacetimes, *Phys. Rev. Lett.* **96**, 071301 (2006); Hawking emission of gravitons in higher dimensions: Non-rotating black holes, *J. High Energy Phys.* **02** (2006) 021; S. Creek, O. Eftimiou, P. Kanti, and K. Tamvakis, Graviton emission in the bulk from a higher-dimensional Schwarzschild black hole, *Phys. Lett. B* **635**, 39 (2006).
- [20] C.M. Harris and P. Kanti, Hawking radiation from a  $(4+n)$ -dimensional rotating black hole, *Phys. Lett. B*

- 633**, 106 (2006); G. Duffy, C. Harris, P. Kanti, and E. Winstanley, Brane decay of a  $(4 + n)$ -dimensional rotating black hole: Spin-0 particles, *J. High Energy Phys.* **09** (2005) 049.
- [21] M. Casals, P. Kanti, and E. Winstanley, Brane decay of a  $(4 + n)$ -dimensional rotating black hole: II. Spin-1 particles, *J. High Energy Phys.* **02** (2006) 051.
- [22] M. Casals, S. Dolan, P. Kanti, and E. Winstanley, Brane decay of a  $(4 + n)$ -dimensional rotating black hole: III. Spin-1/2 particles, *J. High Energy Phys.* **03** (2007) 019; Bulk emission of scalars by a rotating black hole, *J. High Energy Phys.* **06** (2008) 071.
- [23] D. Ida, K. y. Oda, and S. C. Park, Rotating black holes at future colliders: Greybody factors for brane fields, *Phys. Rev. D* **67**, 064025 (2003); Erratum, *Phys. Rev. D* **69**, 049901(E) (2004); Rotating black holes at future colliders: II. Anisotropic scalar field emission, *Phys. Rev. D* **71**, 124039 (2005); Rotating black holes at future colliders: III. Determination of black hole evolution, *Phys. Rev. D* **73**, 124022 (2006).
- [24] S. Creek, O. Efthimiou, P. Kanti, and K. Tamvakis, Greybody factors for brane scalar fields in a rotating black-hole background, *Phys. Rev. D* **75**, 084043 (2007); Greybody factors in a rotating black-hole background: II. Fermions and gauge bosons, *Phys. Rev. D* **76**, 104013 (2007); Scalar emission in the bulk in a rotating black hole background, *Phys. Lett. B* **656**, 102 (2007).
- [25] V. P. Frolov and D. Stojkovic, Quantum radiation from a 5-dimensional rotating black hole, *Phys. Rev. D* **67**, 084004 (2003); H. Nomura, S. Yoshida, M. Tanabe, and K. i. Maeda, The fate of a five-dimensional rotating black hole via Hawking radiation, *Prog. Theor. Phys.* **114**, 707 (2005); E. Jung and D. K. Park, Bulk versus brane in the absorption and emission: 5D rotating black hole case, *Nucl. Phys. B* **731**, 171 (2005); Validity of Emparan-Horowitz-Myers argument in Hawking radiation into massless spin-2 fields, *Mod. Phys. Lett. A* **22**, 1635 (2007); S. Chen, B. Wang, R. K. Su, and W. Y. Hwang, Greybody factors for rotating black holes on codimension-2 branes, *J. High Energy Phys.* **03** (2008) 019.
- [26] H. Kodama, Superradiance and instability of black holes, *Prog. Theor. Phys. Suppl.* **172**, 11 (2008); Perturbations and stability of higher-dimensional black holes, *Lect. Notes Phys.* **769**, 427 (2009); J. Doukas, H. T. Cho, A. S. Cornell, and W. Naylor, Graviton emission from simply rotating Kerr-de Sitter black holes: Transverse traceless tensor graviton modes, *Phys. Rev. D* **80**, 045021 (2009); P. Kanti, H. Kodama, R. A. Konoplya, N. Pappas, and A. Zhidenko, Graviton emission in the bulk by a simply rotating black hole, *Phys. Rev. D* **80**, 084016 (2009).
- [27] A. Flachi, M. Sasaki, and T. Tanaka, Spin polarization effects in micro black hole evaporation, *J. High Energy Phys.* **05** (2009) 031.
- [28] M. Casals, S. R. Dolan, P. Kanti, and E. Winstanley, Angular profile of emission of nonzero spin fields from a higher-dimensional black hole, *Phys. Lett. B* **680**, 365 (2009).
- [29] D. C. Dai and D. Stojkovic, Analytic explanation of the strong spin-dependent amplification in Hawking radiation from rotating black holes, *J. High Energy Phys.* **08** (2010) 016.
- [30] M. O. P. Sampaio, Angular correlations in TeV-gravity black hole events, *J. High Energy Phys.* **03** (2012) 066.
- [31] J. Grain, A. Barrau, and P. Kanti, Exact results for evaporating black holes in curvature-squared Lovelock gravity: Gauss-Bonnet greybody factors, *Phys. Rev. D* **72**, 104016 (2005).
- [32] V. P. Frolov and D. Stojkovic, Black hole radiation in the brane world and recoil effect, *Phys. Rev. D* **66**, 084002 (2002); Black Hole as a Point Radiator and Recoil Effect in the Brane World, *Phys. Rev. Lett.* **89**, 151302 (2002); D. Stojkovic, Distinguishing between the Small ADD and RS Black Holes in Accelerators, *Phys. Rev. Lett.* **94**, 011603 (2005).
- [33] D. C. Dai, N. Kaloper, G. D. Starkman, and D. Stojkovic, Evaporation of a black hole off of a tense brane, *Phys. Rev. D* **75**, 024043 (2007); T. Kobayashi, M. Nozawa, and Y. Takamizu, Bulk scalar emission from a rotating black hole pierced by a tense brane, *Phys. Rev. D* **77**, 044022 (2008).
- [34] R. Jorge, E. S. de Oliveira, and J. V. Rocha, Greybody factors for rotating black holes in higher dimensions, *Classical Quantum Gravity* **32**, 065008 (2015).
- [35] R. Dong and D. Stojkovic, Greybody factors for a black hole in massive gravity, *Phys. Rev. D* **92**, 084045 (2015).
- [36] G. Panotopoulos and A. Rincon, Greybody factors for a nonminimally coupled scalar field in BTZ black hole background, [arXiv:1611.06233](https://arxiv.org/abs/1611.06233).
- [37] Y. G. Miao and Z. M. Xu, Hawking radiation of five-dimensional charged black holes with scalar fields, [arXiv:1704.07086](https://arxiv.org/abs/1704.07086).
- [38] P. Kanti, J. Grain, and A. Barrau, Bulk and brane decay of a  $(4 + n)$ -dimensional Schwarzschild-de Sitter black hole: Scalar radiation, *Phys. Rev. D* **71**, 104002 (2005).
- [39] T. Harmark, J. Natario, and R. Schiappa, Greybody Factors for  $d$ -dimensional black holes, *Adv. Theor. Math. Phys.* **14**, 727 (2010).
- [40] S. F. Wu, S. y. Yin, G. H. Yang, and P. M. Zhang, Energy and entropy radiated by a black hole embedded in de Sitter braneworld, *Phys. Rev. D* **78**, 084010 (2008).
- [41] L. C. B. Crispino, A. Higuchi, E. S. Oliveira, and J. V. Rocha, Greybody factors for nonminimally coupled scalar fields in Schwarzschild-de Sitter spacetime, *Phys. Rev. D* **87**, 104034 (2013).
- [42] P. Kanti, T. Pappas, and N. Pappas, Greybody factors for scalar fields emitted by a higher-dimensional Schwarzschild-de Sitter black hole, *Phys. Rev. D* **90**, 124077 (2014).
- [43] T. Pappas, P. Kanti, and N. Pappas, Hawking radiation spectra for scalar fields by a higher-dimensional Schwarzschild-de Sitter black hole, *Phys. Rev. D* **94**, 024035 (2016).
- [44] P. R. Anderson, A. Fabbri, and R. Balbinot, Low frequency gray-body factors and infrared divergences: Rigorous results, *Phys. Rev. D* **91**, 064061 (2015).
- [45] C. A. Sporea and A. Borowiec, Low energy greybody factors for fermions emitted by a Schwarzschild-de Sitter black hole, *Int. J. Mod. Phys. D* **25**, 1650043 (2016).
- [46] J. Ahmed and K. Saifullah, Greybody factor of scalar field from Reissner-Nordstrom-de Sitter black hole, [arXiv:1610.06104](https://arxiv.org/abs/1610.06104).
- [47] S. Fernando, Bardeen-de Sitter black holes, *Int. J. Mod. Phys. D* **26**, 1750071 (2017).

- [48] P. Boonserm, T. Ngampitipan, and P. Wongjun, Greybody factor for black holes in dRGT massive gravity, [arXiv:1705.03278](#).
- [49] G. W. Gibbons and S. W. Hawking, Cosmological event horizons, thermodynamics, and particle creation, *Phys. Rev. D* **15**, 2738 (1977).
- [50] G. W. Gibbons and S. W. Hawking, Action integrals and partition functions in quantum gravity, *Phys. Rev. D* **15**, 2752 (1977).
- [51] R. Bousso and S. W. Hawking, Pair creation of black holes during inflation, *Phys. Rev. D* **54**, 6312 (1996).
- [52] S. Shankaranarayanan, Temperature and entropy of Schwarzschild–de Sitter space-time, *Phys. Rev. D* **67**, 084026 (2003).
- [53] M. Urano, A. Tomimatsu, and H. Saida, Mechanical first law of black hole spacetimes with cosmological constant and its application to Schwarzschild–de Sitter spacetime, *Classical Quantum Gravity* **26**, 105010 (2009).
- [54] S. Bhattacharya and A. Lahiri, Mass function and particle creation in Schwarzschild–de Sitter spacetime, *Eur. Phys. J. C* **73**, 2673 (2013).
- [55] S. Bhattacharya, A note on entropy of de Sitter black holes, *Eur. Phys. J. C* **76**, 112 (2016).
- [56] H. F. Li, M. S. Ma, and Y. Q. Ma, Thermodynamic properties of black holes in de Sitter space, *Mod. Phys. Lett. A* **32**, 1750017 (2017).
- [57] D. Kubiznak, R. B. Mann, and M. Teo, Black hole chemistry: Thermodynamics with  $\lambda$ , *Classical Quantum Gravity* **34**, 063001 (2017).
- [58] L. J. Romans, Supersymmetric, cold and lukewarm black holes in cosmological Einstein–Maxwell theory, *Nucl. Phys. B* **383**, 395 (1992).
- [59] D. Kastor and J. H. Traschen, Cosmological multi-black hole solutions, *Phys. Rev. D* **47**, 5370 (1993).
- [60] R. G. Cai, Cardy–Verlinde formula and asymptotically de Sitter spaces, *Phys. Lett. B* **525**, 331 (2002); Cardy–Verlinde formula and thermodynamics of black holes in de Sitter spaces, *Nucl. Phys. B* **628**, 375 (2002).
- [61] A. M. Ghezelbash and R. B. Mann, Action, mass and entropy of Schwarzschild–de Sitter black holes and the de Sitter/CFT correspondence, *J. High Energy Phys.* 01 (2002) 005.
- [62] Y. Sekiwa, Thermodynamics of de Sitter black holes: Thermal cosmological constant, *Phys. Rev. D* **73**, 084009 (2006).
- [63] M. Cvetic, G. W. Gibbons, and C. N. Pope, Universal Area Product Formulae for Rotating and Charged Black Holes in Four and Higher Dimensions, *Phys. Rev. Lett.* **106**, 121301 (2011).
- [64] B. P. Dolan, D. Kastor, D. Kubiznak, R. B. Mann, and J. Traschen, Thermodynamic volumes and isoperimetric inequalities for de Sitter black holes, *Phys. Rev. D* **87**, 104017 (2013).
- [65] M. S. Ma, H. H. Zhao, L. C. Zhang, and R. Zhao, Existence condition and phase transition of Reissner–Nordström–de Sitter black hole, *Int. J. Mod. Phys. A* **29**, 1450050 (2014).
- [66] H. H. Zhao, L. C. Zhang, M. S. Ma, and R. Zhao, P–V criticality of higher dimensional charged topological dilaton de Sitter black holes, *Phys. Rev. D* **90**, 064018 (2014).
- [67] L. C. Zhang, M. S. Ma, H. H. Zhao, and R. Zhao, Thermodynamics of phase transition in higher-dimensional Reissner–Nordström–de Sitter black hole, *Eur. Phys. J. C* **74**, 3052 (2014).
- [68] M. S. Ma, L. C. Zhang, H. H. Zhao, and R. Zhao, Phase transition of the higher dimensional charged Gauss–Bonnet black hole in de Sitter spacetime, *Adv. High Energy Phys.* **2015**, 134815 (2015).
- [69] X. Guo, H. Li, L. Zhang, and R. Zhao, Thermodynamics and phase transition in the Kerr–de Sitter black hole, *Phys. Rev. D* **91**, 084009 (2015).
- [70] X. Guo, H. Li, L. Zhang, and R. Zhao, The phase transition of higher dimensional charged black holes, *Adv. High Energy Phys.* **2016**, 7831054 (2016).
- [71] A. Araujo and J. G. Pereira, Entropy in locally–de Sitter spacetimes, *Int. J. Mod. Phys. D* **24**, 1550099 (2015).
- [72] D. Kubiznak and F. Simovic, Thermodynamics of horizons: de Sitter black holes and reentrant phase transitions, *Classical Quantum Gravity* **33**, 245001 (2016).
- [73] J. McInerney, G. Satishchandran, and J. Traschen, Cosmography of KNdS black holes and isentropic phase transitions, *Classical Quantum Gravity* **33**, 105007 (2016).
- [74] H. F. Li, M. S. Ma, L. C. Zhang, and R. Zhao, Entropy of Kerr–de Sitter black hole, *Nucl. Phys. B* **920**, 211 (2017).
- [75] H. Liu and X. h. Meng, Thermodynamics of Schwarzschild–Beltrami–de Sitter black Hole, [arXiv:1611.03604](#).
- [76] B. Pourhassan, S. Upadhyay, and H. Farahani, Thermodynamics of higher order entropy corrected Schwarzschild–Beltrami–de Sitter black hole, [arXiv:1701.08650](#).
- [77] H. Nariai, *Sci. Rep. Tohoku Univ. I.* **35**, 62 (1951).
- [78] R. C. Myers and M. J. Perry, Black holes in higher dimensional space-times, *Ann. Phys. (Berlin)* **172**, 304 (1986).
- [79] C. Molina, Quasinormal modes of  $d$ -dimensional spherical black holes with near extreme cosmological constant, *Phys. Rev. D* **68**, 064007 (2003).
- [80] J. W. York, Jr., Black hole in thermal equilibrium with a scalar field: The back reaction, *Phys. Rev. D* **31**, 775 (1985).
- [81] J. Labbe, A. Barrau, and J. Grain, Phenomenology of black hole evaporation with a cosmological constant, *Proc. Sci.*, HEP2005 (2006) 013.
- [82] M. Bander and C. Itzykson, Group theory and the hydrogen atom, *Rev. Mod. Phys.* **38**, 330 (1966).
- [83] C. Muller, in *Lecture Notes in Mathematics: Spherical Harmonics* (Springer-Verlag, Berlin-Heidelberg, 1966).
- [84] D. N. Page, Particle emission rates from a black hole: 3. Charged leptons from a nonrotating hole, *Phys. Rev. D* **16**, 2402 (1977).
- [85] E. I. Jung, S. H. Kim, and D. K. Park, Absorption cross section for S-wave massive scalar, *Phys. Lett. B* **586**, 390 (2004); Low-energy absorption cross section for massive scalar and Dirac fermion by  $(4 + n)$ -dimensional Schwarzschild black hole, *J. High Energy Phys.* 09 (2004) 005; Proof of universality for the absorption of massive scalar by the higher-dimensional Reissner–Nordström black holes, *Phys. Lett. B* **602**, 105 (2004).
- [86] M. O. P. Sampaio, Charge and mass effects on the evaporation of higher-dimensional rotating black holes, *J. High Energy Phys.* 10 (2009) 008; Distributions of charged massive scalars and fermions from evaporating higher-dimensional black holes, *J. High Energy Phys.* 02 (2010) 042.
- [87] P. Kanti and N. Pappas, Emission of massive scalar fields by a higher-dimensional rotating black-hole, *Phys. Rev. D* **82**, 024039 (2010).